Article

Sensitivity of the Penman–Monteith Reference Evapotranspiration Equation to Meteorological Variables for Puerto Rico

Michelle Irizarry-Ortiz [1],* and Eric W. Harmsen [2]

[1] U.S. Geological Survey, Caribbean-Florida Water Science Center, Orlando, FL 32826, USA
[2] Agricultural and Biosystems Engineering Department, University of Puerto Rico, Mayaguez, PR 00681, USA
* Correspondence: mirizarry-ortiz@usgs.gov; Tel.: +1-407-803-5533

Abstract: Spatiotemporal variations in reference evapotranspiration (ET_o) are sensitive to the meteorological data used in its estimation. The sensitivity of the ASCE standardized ET_o equation to meteorological variables from GOES-PRWEB dataset was evaluated for the island of Puerto Rico. Island wide, ET_o is most sensitive to daily mean relative humidity (RH_{mean}), followed by solar radiation, daily maximum (T_{max}) and minimum (T_{min}) air temperatures, and wind speed with average absolute relative sensitivity coefficients (SCs) of 0.98, 0.57, 0.50, 0.27, and 0.12, respectively. The derived SCs guided the prioritization of bias correction of meteorological data for ET_o estimation from two downscaled climate models (CNRM and CESM). The SCs were applied to evaluate how meteorological variables contribute to model errors and projected future changes in ET_o from 1985–2005 to 2040–2060 at irrigated farms in the south. Both models project a 5.6% average increase in annual ET_o due to projected increases in T_{max} and T_{min} and a decrease in RH_{mean}. Despite ET_o being most sensitive to relative changes in RH_{mean}, the contributions from RH_{mean}, T_{max}, and T_{min} to future changes in ET_o are similar. CESM projects increases in ET_o in March, November, and December, increasing the potential for crop water stress. Study limitations are discussed.

Keywords: evapotranspiration; evaporation; transpiration; water use; water balance; Puerto Rico; sensitivity analysis; climate change; WRF; GOES-PRWEB

1. Introduction

Accurate quantification of evapotranspiration (*ET*) is critical to water resource management and planning, especially in the semi-arid southern part of the island of Puerto Rico where agriculture is dependent on irrigation. Currently, the island only produces 15% of the food consumed by residents [1]. Compared to most of the U.S., where agricultural irrigation was the primary freshwater withdrawal in 2015, irrigation withdrawals from surface water and groundwater sources in Puerto Rico accounted for only about 12% of the total freshwater withdrawals in 2015 [2]. Because agricultural production has declined since the 1960s and urbanization encroached into agricultural lands, an increasing proportion of the island's surface-water withdrawals have been for domestic water supply. In the south, canals that were built primarily to supply irrigation water to agricultural lands are now increasingly being used for public water supply. Increasing competition among water users has limited the capacity for recovery of the agricultural sector [3] by reducing the availability of water supplies for future agricultural production [4]. This may hinder the island's attempts to achieve food sovereignty which is also being threatened by climate change [5].

The island has historically been subject to periods of drought which have adversely affected the agricultural sector. Since the turn of the century, an extreme drought occurred during 2014–2016 and severe drought conditions occurred again in 2019–2022 [6]. A 2013–2016 Caribbean-wide drought was partly linked to 2015–2016 El Niño conditions,

but analysis by Herrera et al. [7] suggests that climate change may have accounted for ~15–17% of the drought severity and/or ~7% of its spatial extent. Downscaled climate models project increased drought intensity and frequency in the future as a result of climate change [8,9]. Therefore, understanding potential future changes in rainfall and actual *ET* from crops is critical for water managers and planners to better prepare for the future. Actual *ET* depends on various factors, including atmospheric evaporative demand, which is quantified via reference evapotranspiration (ET_o), soil water availability, crop physiology, and crop management factors.

The American Society of Civil Engineers (ASCE) has defined a standardized grass-reference Penman–Monteith (P-M) evapotranspiration equation [10] to estimate ET_o on a daily timestep for short grass. When applied on a daily timestep, the ASCE standardized ET_o equation is the same as the Food and Agriculture Organization paper number 56 (FAO-56) P-M equation [11]. Understanding spatiotemporal variations in ET_o requires understanding the sensitivity of standardized equations to each meteorological variable used in its estimation. For this purpose, a sensitivity analysis of the ASCE standardized ET_o equation is performed for Puerto Rico. This involves the computation of non-dimensional relative sensitivity coefficients (SCs) of the ASCE standardized ET_o equation to each of the basic meteorological variables used in its estimation. When combined with a measure of the variability or measurement/estimation error in the basic meteorological variables, the SCs could be used to define monitoring priorities among the variables. ET_o may be sensitive to a particular variable but if that variable varies little in time and if it can be measured or estimated precisely, then the variable will not influence ET_o estimates significantly.

Gong et al. [12], and McKenney and Rosenberg [13] discuss difficulties in comparing results of ET_o sensitivity analysis from the literature, including the use of different ET_o models, parameterizations and meteorological variables, spatiotemporal scales, climatic settings, and SC definitions (i.e., absolute versus relative). The studies discussed hereafter are limited to those where the sensitivity of ET_o to various meteorological variables was determined based on the ASCE or the FAO-56 grass-reference P-M equations. For example, Irmak et al. [11] performed a sensitivity analysis of the ET_o equation at various U.S. locations computing absolute SCs numerically. They found that ET_o is most sensitive to vapor pressure deficit (VPD) at all the U.S. locations evaluated, but that sensitivity to solar radiation (R_s) dominates during the summer months at humid locations (Ft. Pierce, Florida with ~1200 mm of annual precipitation and at Rockport, Missouri with ~800 mm of annual precipitation). Debnath et al. [14] computed absolute SCs for ET_o at five stations in different agroecological regions of India where annual precipitation ranges from 680 to 1500 mm. They found ET_o to be most sensitive to either R_s or 2 m wind speed (u_2), and least sensitive to daily mean relative humidity (RH_{mean}) and daily minimum air temperature (T_{min}) with significant spatiotemporal variation in SCs.

Gong et al. [12] computed relative SCs for ET_o at meteorological stations in the Yangtze River Basin in China, where annual precipitation ranges from 400 to 1600 mm [15]. They found that RH_{mean} was the most sensitive variable, followed by R_s, daily mean air temperature (T_{mean}), and u_2. Seasonal and regional variations in sensitivity were observed. Furthermore, they found that the sensitivity of ET_o to a meteorological variable depended on other variables. For example, although the lower and middle regions of the Yangtze River Basins have similar RH_{mean} year round, the sensitivity of ET_o to changes in RH_{mean} was higher in the Lower basin region, where wind speeds are higher. Similarly, Liu et al. [16] derived relative SCs for ET_o at meteorological stations in the Yellow River Basin in China, which is more arid than the Yangtze River Basin and has annual precipitation of 372–671 mm. They found that R_s was the most sensitive variable in general, followed by RH_{mean}, T_{mean}, and u_2 at the basin scale. Biazar et al. [17] computed relative SCs for ET_o at meteorological stations in a humid region of Iran with annual precipitation of 1000–1850 mm and relative humidity exceeding 85% throughout the year. They found that the most sensitive parameter for ET_o was T_{max} and the least sensitive was T_{min}. Emeka et al. [18] evaluated the relative sensitivity of ET_o at seven distinct agroecological zones in Nigeria. They found that overall ET_o was

most sensitive to RH_{mean}, followed by R_s, T_{max}, u_2, and $T_{min.}$ However, there was significant spatiotemporal variation in sensitivity. In the south of Nigeria, which has a tropical rainforest climate with annual precipitation of 1200–3000 mm, ET_o was most sensitive to RH_{mean} and R_s and least sensitive to u_2. Meanwhile, in the north (annual precipitation of 400–1100 mm), the maximum sensitivity was for T_{max} and the minimum for T_{min}. For the very arid region of the Ejina Oasis in northwest China (annual precipitation less than 50 mm), Hou et al. [19] found that the relative sensitivity of ET_o is highest for R_s, followed by T_{mean}, u_2, and RH_{mean}.

The SCs can also be used to understand past historical and projected future changes in ET_o. Luo et al. [20] performed a sensitivity analysis of the ASCE standardized ET_o equation to understand meteorological drivers of historical trends (mainly increasing) in ET_o in the Yanhe River Basin in China. Liu et al. [16] performed a sensitivity analysis of ET_o in the Yellow River Basin in China to understand temporal trends in ET_o in different regions of the basin. They found that positive trends in the upper, middle, and whole Yellow River Basin resulted from a significant increasing trend in T_{mean} and a decreasing trend in RH_{mean}. Wang et al. [21] used sensitivity analyses to understand the causes of historical decreases in pan evaporation over China, also called the "pan evaporation paradox". The "pan evaporation paradox," first discovered by Peterson et al. [22], was observed for decades in the late 20th century in many areas of the globe and contrasts with the general expectation that atmospheric evaporative demand would increase under climate change as temperatures warm. Similar declining trends in reference and potential evapotranspiration were observed in many areas of the globe during the same period. Wang et al. [21] summarized the contribution of different meteorological variables to reductions in pan evaporation observed in many regions of the globe based on the attribution method proposed by Roderick et al. [23], which is essentially a sensitivity analysis of a pan evaporation equation. Wang et al. [21] found that changes in R_s, u_2, and RH_{mean} overcompensate for the positive contributions of increasing air temperatures on pan evaporation, which resulted in a net decrease in pan evaporation in China and many regions of the globe. However, an evaluation of output from general circulation models (GCMs) from the Coupled Model Intercomparison Phase 5 indicates that the evaporation paradox will not continue into the future, at least in China. McKenney and Rosenberg [13] show that future changes in potential evapotranspiration derived from GCM output using different methods may vary in magnitude and, in some cases, in sign depending on the estimation method used.

Our main objective in deriving SCs for Puerto Rico is to guide the prioritization of bias correction of meteorological output for ET_o estimation from dynamically downscaled climate projections for Puerto Rico by Bowden et al. [9] for the historical period 1985–2005 and the future period 2040–2060. The derived SCs are also applied to evaluate the drivers of potential future changes in ET_o in Puerto Rico. Of particular interest are potential future changes to agricultural water demand on irrigated farms and golf courses on the island, which are a function of future projected changes in precipitation and ET_o. Bias-corrected ET_o can be used to drive models (i.e., soil-moisture water-balance models [2]) to estimate potential future changes to agricultural irrigation requirements on the island.

2. Materials and Methods

2.1. Study Area

The study area consists of the main island of the Commonwealth of Puerto Rico, which has a wide range of climate types. Precipitation ranges from 800 mm/year in the subtropical dry forest on the south coast to over 4300 mm/year [24] in the subtropical rainforest of El Yunque, which is part of the Sierra de Luquillo on the northeast of the island (Figure 1). The spatial variability of rainfall results from easterly to northeasterly winds interacting with the local orography. Large rainfall amounts fall north [24] of the mountain range, which runs predominantly east–west over central portions of the island known as the Cordillera Central and the Sierra de Cayey, which runs southeastward on the eastern side of the island. The rainfall maximum occurs over the Sierra de Luquillo mountains

in the northeast where the El Yunque rainforest is located. A westerly sea-breeze front develops on the western side of the island, which converges with the predominant easterly winds, resulting in strong convection and high rainfall amounts in the northwest part of the island. A rain shadow occurs over most of the southern coast of the island. Rainfall has a bimodal distribution with the highest rainfall in May–early June and late July–November. A mid-summer drought (MSD) develops in late June through early July and, based on climate model simulations, has been found to be the combined result of increased aerosol concentrations from Saharan dust events and changes in vertical wind shear [25].
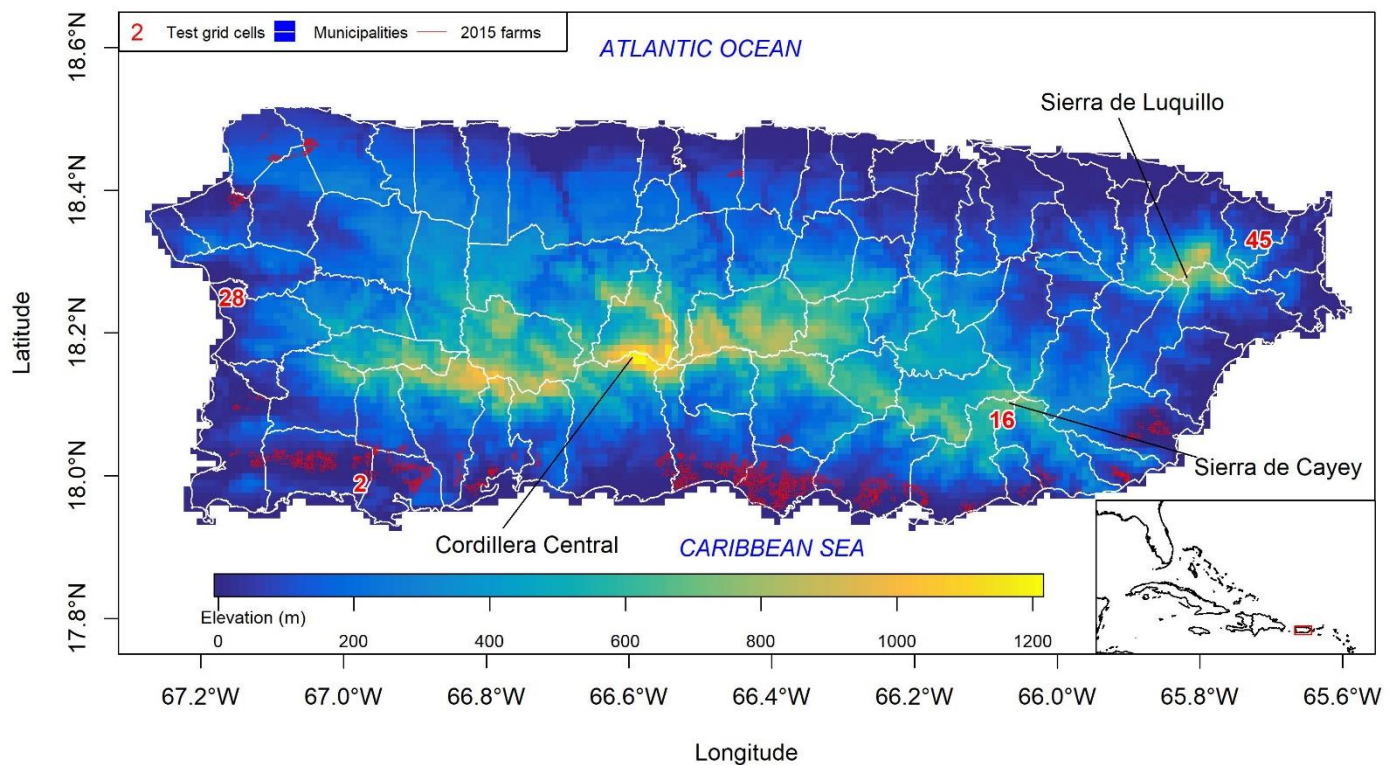

Figure 1. Study area consisting of the main island of Puerto Rico. Elevation in meters is shown. The white lines show the boundaries of the municipalities in Puerto Rico, and the red lines show the boundaries of irrigated farms in 2015. Numbers indicate the location of Geostationary Operational Environmental Satellite-Puerto Rico Water and Energy Balance (GOES-PRWEB) 1 km-scale grid cells at which timeseries of sensitivity coefficients will be presented in detail. Base for main map from 1:20,000 USGS Digital Line Graphs municipality boundaries. Base for inset map is from version 1.4.0 of Natural Earth data, country boundaries 1:10 m. Both are in geographic coordinate system and World Geodetic System 1984 datum.

Low relative humidity, high temperatures, high wind speed, and high incoming solar radiation on the south coast result in high atmospheric evaporative demand compared to rainfall. The south-coast region is characterized by alluvial floodplains with highly fertile soils (mollisols), which are rich in organic matter and minerals [26]. This has made the region suitable for agriculture, which, owing to the relatively low annual rainfall, is dependent on irrigation. Of particular interest to water managers are potential future changes in water availability and water use across the island [4]. There is increasing concern about potential future conflicts among domestic and agricultural water uses on the southern coast of the island [4]. Therefore, it is important to quantify potential future agricultural water demand on irrigated farms and golf courses on the island, which are predominantly located in this southern region (Figure 1; [27]). Agriculture also occurs in the interior mountainous parts of the island, which receive high amounts of rainfall during

the year so as not to require irrigation, but these areas may also be subjected to reductions in rainfall in the future [9].

2.2. Data

2.2.1. Gridded Historical Data

The Geostationary Operational Environmental Satellite-Puerto Rico Water and Energy Balance (GOES-PRWEB) dataset [28] provides daily gridded data for water and energy budget components at a 1 km resolution over Puerto Rico for the period 2009–2020. GOES-PRWEB provides estimates of daily rainfall, actual evapotranspiration, reference evapotranspiration (ET_o) based on the FAO-56 (or ASCE) P-M equation (Equation (1) in Section 2.3), as well as data for five basic meteorological variables that are used in estimating ET_o: daily maximum (T_{max}) and minimum (T_{min}) air temperature at 2 meter height, daily mean relative humidity (RH_{mean}), daily mean incoming solar radiation at the land surface (R_s), and 2 m-height wind speed (u_2). Appendix S1 in Supplementary Materials summarizes the GOES-PRWEB computation of ET_o from these five basic variables. GOES-PRWEB estimates actual ET based on the surface energy balance equation, as described by Harmsen et al. [28]. The GOES-PRWEB estimated ET_o and its driving meteorological variables have been validated by Mecikalski and Harmsen [29] and Harmsen et al. [28,30] at a few stations on the island, supporting the use of GOES-PRWEB ET_o in this study. For this study, GOES-PRWEB data for the period 2009–2017 is used.

The high-resolution regional statistical downscaled GPCC v7 for the Caribbean dataset (Herrera-Ault; [7,31]) provides estimates of monthly potential evapotranspiration based on the FAO-56 P-M equation [32] at an approximate resolution of 4 km. Although these data are referred to as potential evapotranspiration, Herrera and Ault [31] mention that this dataset refers to evapotranspiration from an idealized grass surface, that is, ET_o. ET_o data from this dataset show higher values than GOES-PRWEB from December to April and lower values than GOES-PRWEB the rest of the year. Besides T_{max} and T_{min}, Herrera-Ault does not provide data for the remaining variables required for ET_o estimation using the FAO-56 P-M equation. This lack of availability of all the meteorological data needed for ET_o estimation makes it impossible to investigate the causes of the differences in seasonality between the two datasets.

2.2.2. WRF Dynamically Downscaled Climate Change Projections

Bowden et al. [9] used the Weather Research and Forecasting (WRF) model to dynamically downscale historical (1985–2005) and future climate projections (2040–2060) for Puerto Rico and the U.S. Virgin Islands under the greenhouse gas emission scenario RCP8.5 for two GCMs from the Coupled Model Intercomparison Project phase 5 (CMIP5): (1) the Community Climate System Model (CCSM4 or CESM) and (2) the Centre National de Recherches Météorologiques-CERFACS (CNRM). Hourly output from the innermost model domain (domain 3 at 2-km resolution) was downloaded from the Bowden et al. [33], converted from Greenwich Meridian Time to local time (Atlantic Standard Time), and the five basic daily meteorological variables used for ET_o estimation in GOES-PRWEB were computed and bilinearly interpolated to the 1-km GOES-PRWEB grid. Appendix S2 in Supplementary Materials has a description of the computation of daily meteorological data from hourly data.

2.3. Methods

Actual ET depends on various factors, including atmospheric evaporative demand, soil water availability, crop physiology, and management practices. Absent actual ET data, crop potential evapotranspiration (ET_c) is often computed based on the potential evapotranspiration from a reference crop, typically grass or alfalfa, which is called reference evapotranspiration. Grass reference evapotranspiration is denoted as ET_o and refers to a crop assumed to be 0.12 m in height, with an albedo of 0.23 and a daily surface resistance of 70 s/m [10]. Crop coefficients (K_c) are often used as multipliers to convert ET_o to ET_c

(i.e., $ET_c = K_c ET_o$). ET_o accounts primarily for weather conditions (i.e., atmospheric evapo-rative demand), and K_c accounts for the characteristics of a specific crop with respect to the reference grass under fully watered conditions [32]. Therefore, the crop coefficients incorporate many factors that distinguish a particular crop from the reference grass, including planting date, plant growth stage, leaf area, albedo or reflectivity, canopy resistance, soil and climate conditions, evaporation from soil, and crop management practices, among others [32]. In conditions of insufficient rainfall or irrigation and a deficit in soil moisture, the actual combined soil evaporation and plant transpiration (actual ET) will be lower than ET_c. GOES-PRWEB estimates actual ET based on the surface energy balance equation, as described by Harmsen et al. [28]. In modeling applications, where actual ET cannot be esti-mated a priori but depends on the simulated hydrology, actual ET is often estimated from ET_o using modified crop coefficients, which not only account for crop-type differences but also for water availability. Water stress coefficients, which are often defined as a function of soil water content and/or depth to the water table, can be applied as multiplicative correc-tion factors to the standard crop coefficients for well-watered conditions [32] to estimate actual ET.

The ASCE standardized grass-reference Penman–Monteith evapotranspiration equa-tion [10] for short grass on a daily timestep is given by:

$$ET_o = \frac{0.408 \, \Delta \, (R_n - G) + \gamma \frac{900}{T+273} u_2 (e_s - e_a)}{\Delta + \gamma(1 + 0.34u_2)}, \tag{1}$$

where ET_o is the daily reference evapotranspiration (mm/day), R_n is the net radiation at the crop surface (MJ/m^2/day), G is the soil heat flux density at the soil surface (MJ/m^2/day), which is generally small compared to R_n beneath a fully vegetated reference surface, and hence, neglected for daily timesteps, T is the mean daily air temperature at 2 meters (°C), u_2 is the mean daily wind speed at 2 meters (m/s), e_s is the saturation vapor pressure at 2 meters (kPa), e_a is the mean actual vapor pressure at 2 meters (kPa), Δ is the slope of the saturation vapor pressure–temperature curve (kPa/°C), and γ is the psychrometric constant (kPa/°C). Appendix S1 summarizes how each of these variables are estimated from five basic meteorological variables defined hereafter and available in GOES-PRWEB. When applied on a daily timestep, the ASCE standardized ET_o equation is the same as the Food and Agriculture Organization paper number 56 (FAO-56) P-M equation [11].

A sensitivity analysis was performed for the ASCE ET_o equation to determine the sensitivity of ET_o to each of the five basic meteorological variables listed above. Neglecting higher-order terms, the sensitivity of ET_o to changes (or errors) in each of the individual basic meteorological variables is quantified by means of non-dimensional relative sensitivity coefficients [34]:

$$S_{V_i} = \frac{\partial ET_o}{\partial V_i} \times \frac{V_i}{ET_o}, \tag{2}$$

where V_i is one of five basic meteorological variables (T_{max} in °C, T_{min} in °C, RH_{mean} in %, R_s in MJ/m^2/day, or u_2 in m/s), i is the index for the variable (1–5), S_{V_i} is the relative SC for variable V_i, and $\frac{\partial ET_o}{\partial V_i}$ is the partial derivative of ET_o with respect to V_i. A positive (negative) SC for a variable indicates that ET_o will increase (decrease) as the variable increases and can be visualized as the slope of the tangent at the origin of the sensitivity curve. The derivatives, $\frac{\partial ET_o}{\partial V_i}$, were derived analytically (Appendix S3 of the Supplementary Materials) and also derived numerically, and their linearity assessed by computing and plotting the percentage change in ET_o due to +/− 5, 10, 15, 20, and 25% change in V_i alone. This is done by changing the value of the variable of interest at each particular location on each day by a given percentage while keeping the remaining variables fixed at their observed value and computing the resulting change in ET_o as a percentage. For RH_{mean}, only negative percent changes were evaluated in order to keep it from exceeding 100%. It is expected that the analytically derived SCs will be closest to those derived based on +/− 5% perturbations for a particular variable. The range of variation in a meteorological variable over which

the slope of the sensitivity curve is linear is also assessed. The larger the range of linearity, the smaller the error incurred when applying the point SCs over large changes in the meteorological variable.

The SCs are estimated based on daily GOES-PRWEB gridded meteorological data for the period 2009–2017 and averaged for each day or month of the year to obtain the average annual cycle of the SCs for each variable of interest at each grid cell. Timeseries of average SCs by day of the year will be presented at four representative locations on the island (Figure 1) that capture most of the distinct patterns of variation in the SCs as well as maps of long-term monthly average SCs.

When combined with a measure of the variability or measurement/estimation error in the basic meteorological variables, the SCs could be used to define monitoring priorities among the variables. The SCs could also be used to guide the prioritization of bias correction of meteorological output for ET_o estimation from climate models. When combined with projections of the percent change in the basic meteorological variables, the SCs can aid in understanding past trends and future projected changes in ET_o derived from observations and climate model output. Based on the chain rule, which helps differentiate composite functions, the combined contributions of fractional changes or errors in the basic meteorological variables to fractional changes or errors in ET_o can be approximated by:

$$\frac{dET_o}{ET_o} = \sum_i \left(S_{V_i} \times \frac{dV_i}{V_i} \right) + error = \sum_i \left(\frac{\partial ET_o}{\partial V_i} \times \frac{V_i}{ET_o} \times \frac{dV_i}{V_i} \right) + error, \qquad (3)$$

where *error* is the approximation error.

An example application of the SCs and Equation (3) to understanding biases and potential future changes in ET_o from 1985–2005 to 2040–2060 based on the dynamically downscaled climate projections for Puerto Rico by Bowden et al. [9] will be presented in this paper. Of particular interest are potential future changes to agricultural water demand on irrigated farms on the island, which are a function of future projected changes in precipitation and evaporative demand (ET_o). As of the year 2015, most irrigated farms are located in the fertile semi-arid southern coast of Puerto Rico (Figure 1; [27]). The average annual cycle of the SCs and the contribution of projected changes in each of the basic meteorological variables to projected changes in ET_o were calculated for all model grid cells whose center is located within a 2015 irrigated farm. No comprehensive gridded meteorological dataset including daily data for all the basic meteorological variables used in estimating ET_o has been located for the simulated historical period 1985–2005; therefore, GOES-PRWEB data for 2009–2017 is used to examine potential biases in ET_o calculated from downscaled model output and the contribution of individual meteorological variables to those biases.

Finally, the Pearson correlation coefficient (*r*) between long-term monthly average maps of SCs, the five basic meteorological variables, the aerodynamic and energetic components of ET_o and their fractions ($ET_{o,energetic}$, $ET_{o,aerodynamic}$, $ET_{o,energetic\ fraction}$, $ET_{o,aerodynamic\ fraction}$, respectively, given by Equations (S1.1)–(S1.5) in the Supplementary Materials), rainfall, and elevation will be presented. The Pearson correlation coefficient is a measure of the strength of the linear association between two sets of data and will be used here to better understand how different variables affect or are correlated with ET_o. Because the correlation coefficient is calculated between all the monthly maps, it captures both temporal and spatial correlations between the different fields. In the discussion, the correlation (or anti-correlation) between variables is considered moderate for absolute values of *r* of 0.50–0.69, high for absolute values of *r* of 0.70–0.89, and very high for absolute values of *r* of 0.90–1.00.

3. Results

Spatiotemporal variations in rainfall, *ET*, and other components of the hydrologic cycle in Puerto Rico will be presented as maps and seasonal and annual plots. Results of the sensitivity analysis will be presented as long-term (2009–2017) monthly average maps of SCs and timeseries of SCs at various locations. Results from the application of

SCs to understand model biases and projected future changes in ET_o based on dynamically downscaled climate model output will also be presented.

3.1. Spatiotemporal Variations in Rainfall and ET

On the basis of GOES-PRWEB data [28], it was found that annual rainfall (Figure 2a) and annual actual *ET* (Figure 2b) are similar in magnitude across large portions of the island. About 65% of rainfall on average island wide, and upwards of 90% in the south coast, returns to the atmosphere as evapotranspiration on an average year (Figure 2c). Only a small fraction of annual rainfall recharges the shallow aquifer (Figure 2e), while the fraction of annual rainfall that generates runoff is higher in areas with higher rainfall, such as on the central northwest part of the island and on the Sierra de Luquillo in the northeast (Figure 2f). Annual atmospheric evaporative demand, as quantified by ET_o, is more than twice as high as annual rainfall over the south coast of Puerto Rico (Figure 2d), where agriculture has to rely on irrigation to meet the atmospheric evaporative demand. Low relative humidity, high temperatures, high wind speed, and high incoming solar radiation on the south coast result in high ET_o compared to rainfall.
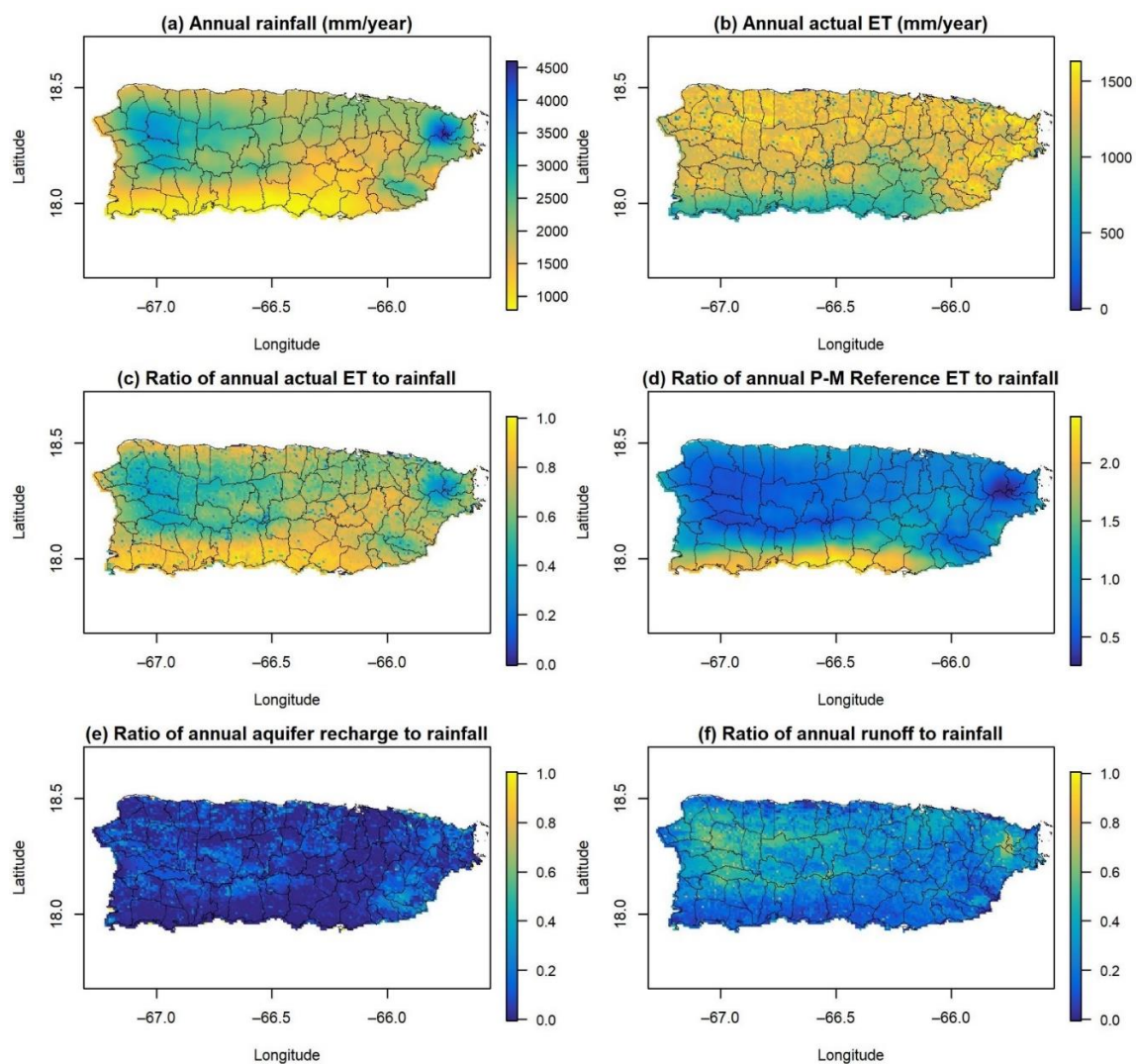

Figure 2. (**a**) Annual rainfall (mm/year); (**b**) annual actual *ET* (mm/year); (**c**) ratio of annual actual *ET* to rainfall; (**d**) ratio of annual Penman–Monteith ET_o to rainfall; (**e**) ratio of annual aquifer recharge to rainfall; and (**f**) ratio of annual runoff to rainfall for Puerto Rico based on Geostationary Operational Environmental Satellite-Puerto Rico Water and Energy Balance (GOES-PRWEB) data for 2009–2017. The black lines show the location of the municipalities in Puerto Rico.

Figure 3a,b illustrate the annual cycle of monthly rainfall and ET_o and Figure 3c illustrates the interannual variability of ET_o at the 2015 irrigated farm locations. The bimodal distribution of rainfall is evident in Figure 3a, with the highest rainfall in May–early June and late July–November. The mid-summer drought (MSD) that develops in late June through early July is also evident. The annual cycle of monthly ET_o (Figure 3b) from GOES-PRWEB with peak values in July appears to match station-based estimates of ET_o in Harmsen et al. [35] better than the Herrera-Ault ET_o which peaks in March. This justifies our use of GOES-PRWEB ET_o in this study.
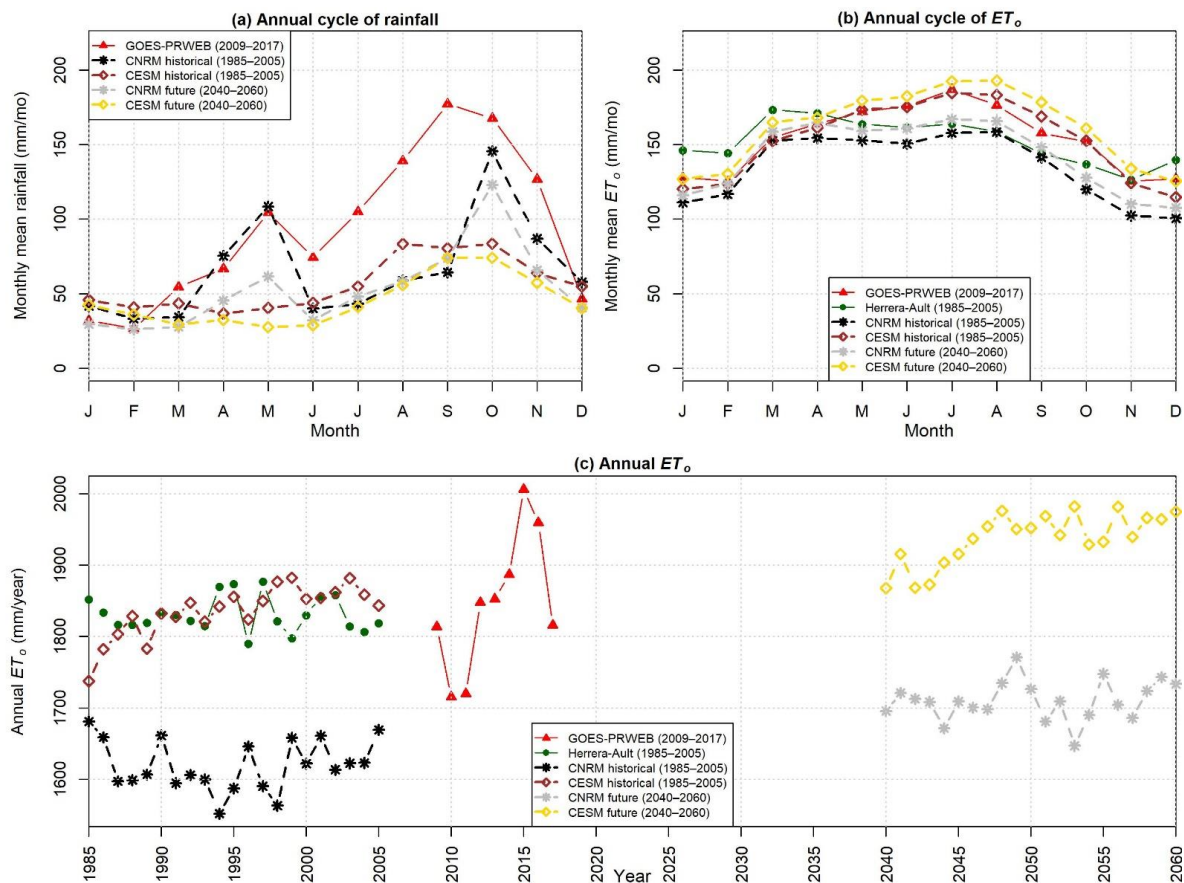
Figure 3. (**a**) Annual cycle of rainfall (mm/mo.); (**b**) annual cycle of ET_o (mm/mo.); (**c**) annual ET_o (mm/year) from Geostationary Operational Environmental Satellite-Puerto Rico Water and Energy Balance (GOES-PRWEB), Herrera-Ault dataset, and WRF dynamically downscaled climate models at the 2015 irrigated farm locations.

3.2. Sensitivity Coefficients

Sensitivity coefficients for ET_o, with respect to each of the five basic meteorological variables, were computed analytically and numerically at each GOES-PRWEB grid cell for each day in the period 2009–2017. Maps of the long-term (2009–2017) monthly average sensitivity coefficients derived analytically are shown in Figures 4–8. The maps derived numerically for a +/− 5% change in each meteorological variable (not shown) are very similar, corroborating the analytical calculations. The SC for RH_{mean} is negative because an increase in atmospheric water content reduces ET_o. To make the SC for RH_{mean} of comparable magnitude to the SC of the other meteorological variables, it is multiplied by −1 in Figure 4. Island wide, ET_o is most sensitive to RH_{mean}, followed by R_s, T_{max}, T_{min}, and u_2, with average absolute relative SCs of 0.98, 0.57, 0.50, 0.27, and 0.12, respectively. This overall ranking of sensitivities is similar to that found by Emeka et al. [18] based on relative sensitivities for the tropical rainforest climate of southern Nigeria, where precipitation ranges from 1200 to 3000 mm per year, similar to the range of annual precipitation in Puerto

Rico (Figure 2a). The only exception is that in southern Nigeria, ET_o was found to be most sensitive to R_s followed by RH_{mean} in the non-monsoon season. The ranking of sensitivities also agrees well with that obtained by Gong et al. [12] for the Yangtze River Basin in China, especially during winter when the sensitivity to RH_{mean} is higher than that of R_s and T_{mean}. Annual precipitation ranges from 400 in the upper Yangtze River Basin to 1600 mm in the lower basin [15]. Only the middle and lower portions of the Yangtze River Basin have annual precipitation comparable to that of some regions in Puerto Rico (Figure 2a).
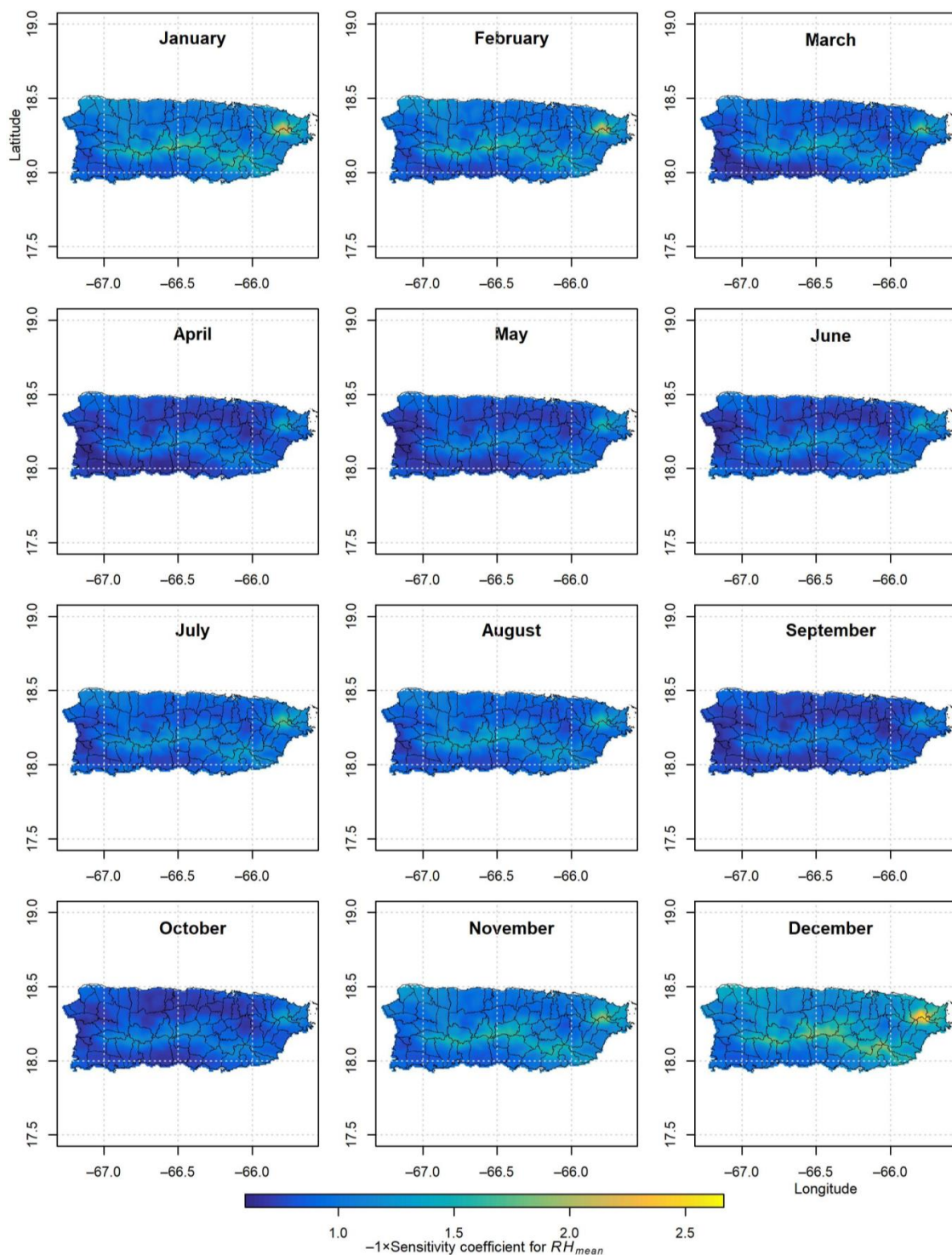
Figure 4. Long-term (2009–2017) monthly average sensitivity coefficients, multiplied by −1, for mean relative humidity (RH_{mean}). The black lines show the location of the municipalities in Puerto Rico.
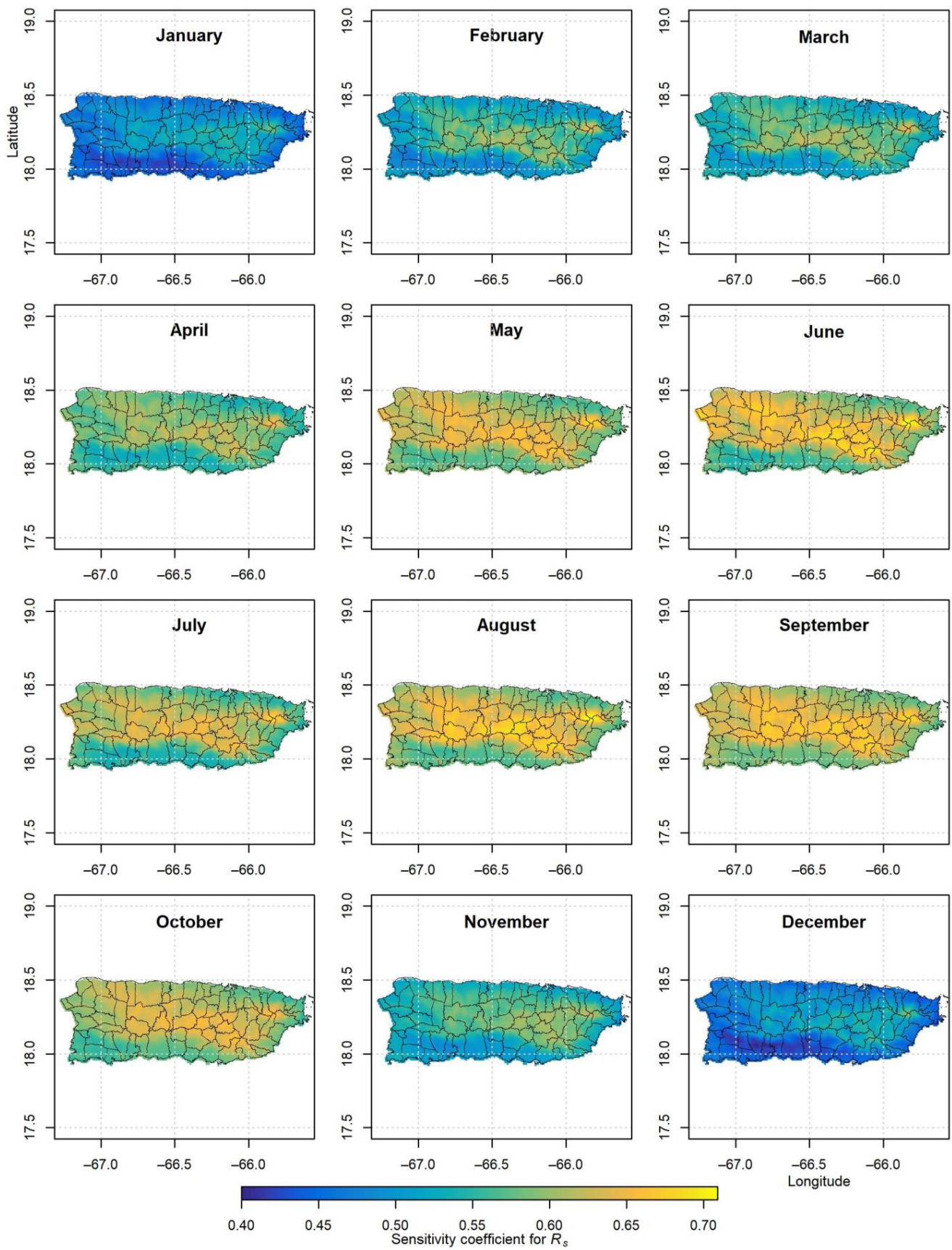
Figure 5. Long-term (2009–2017) monthly average sensitivity coefficients for solar radiation (R_s). The black lines show the location of the municipalities in Puerto Rico.
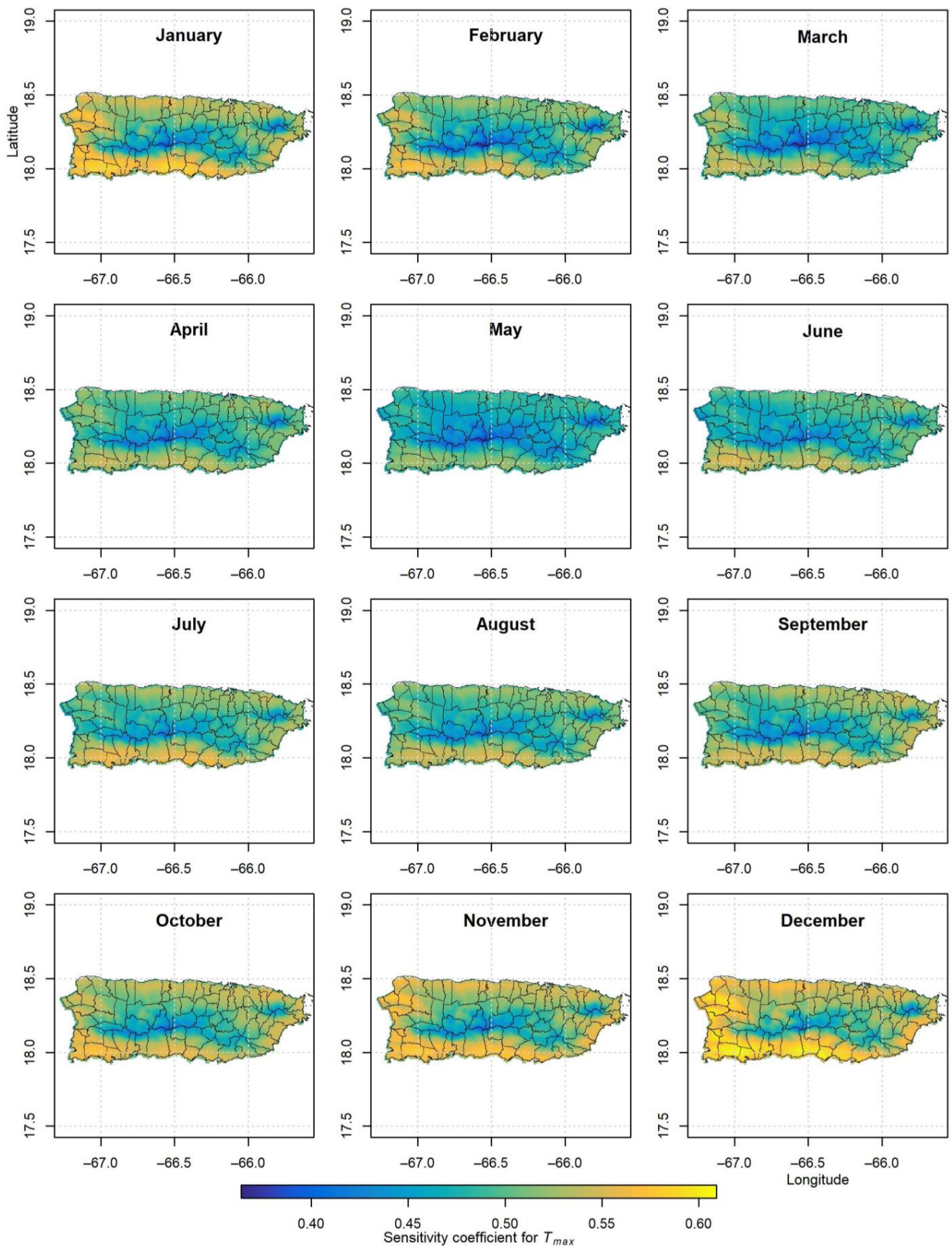
Figure 6. Long-term (2009–2017) monthly average sensitivity coefficients for daily maximum air temperature (T_{max}). The black lines show the location of the municipalities in Puerto Rico.
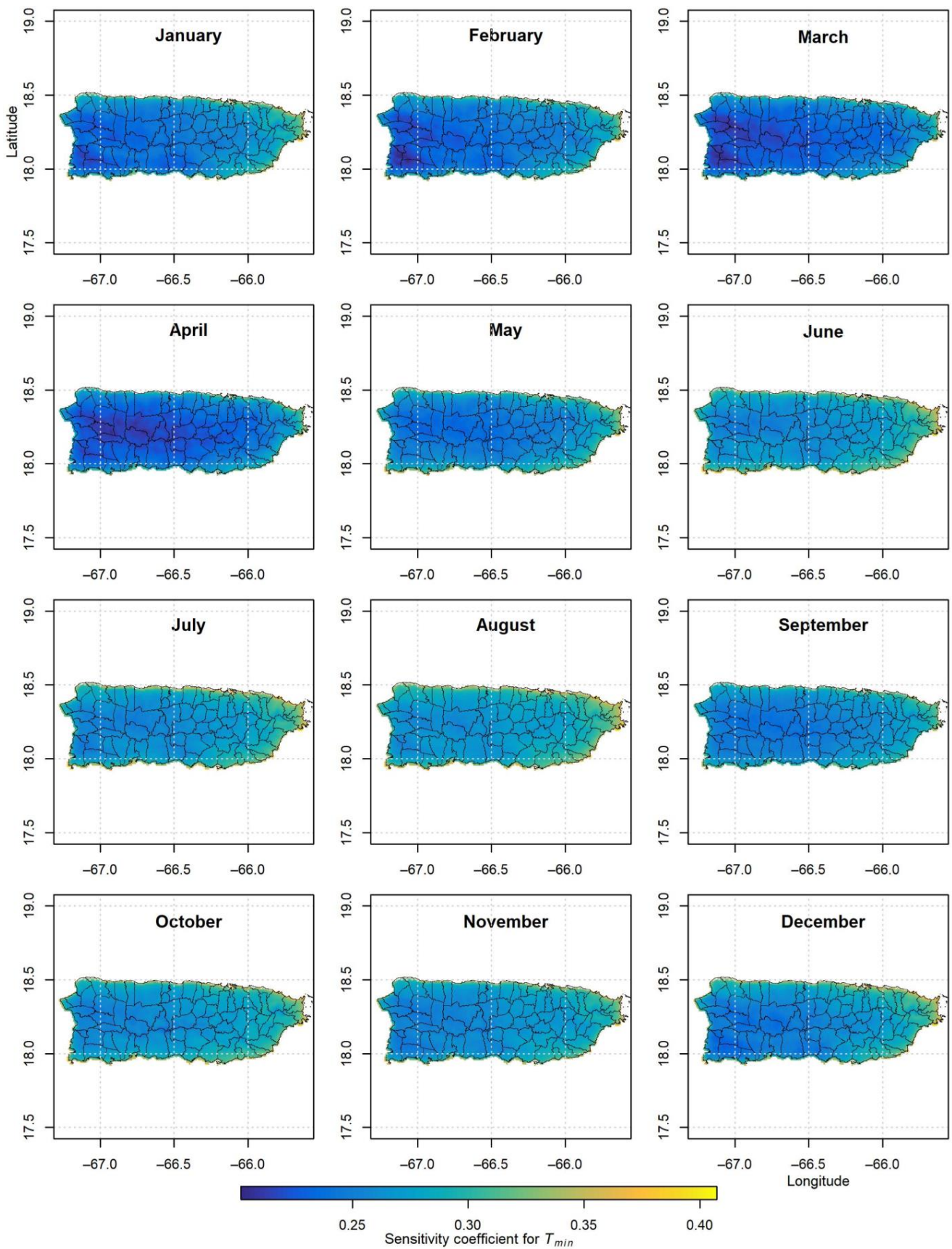
Figure 7. Long-term (2009–2017) monthly average sensitivity coefficients for daily minimum air temperature (T_{min}). The black lines show the location of the municipalities in Puerto Rico.
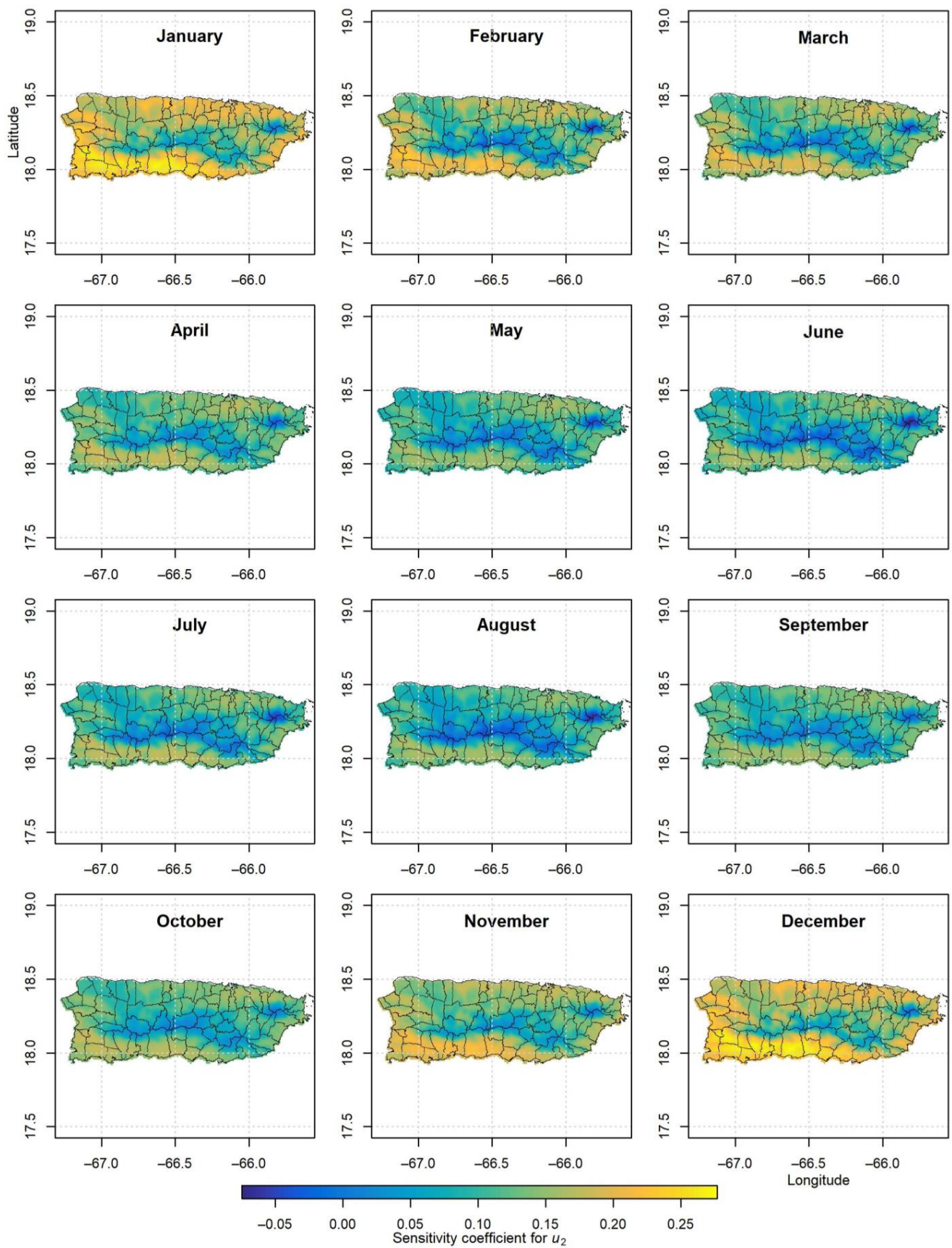
Figure 8. Long-term (2009–2017) monthly average sensitivity coefficients for 2 m wind speed (u_2). The black lines show the location of the municipalities in Puerto Rico.

Timeseries of SCs by day of the year averaged over the period 2009–2017 at the chosen four GOES-PRWEB grid cell locations (cells 2, 16, 28, 45; Figure 1) are shown in Figure 9. In addition, the average timeseries of SCs for the location of the farms as of 2015 shown in Figure 1 is also shown in Figure 9. The SC for RH_{mean} (Figures 4 and 9) dominates the sensitivity of ET_o throughout most of the island, except for the western side of the island (cell 28 in Figures 1 and 9), where the SC for R_s is as or more dominant during the summer. The SC for RH_{mean} has a large amplitude annual cycle, especially along the Cordillera Central mountains and the Sierra de Luquillo with larger values and less day-to-day variability in the dry season than in the wet season. Coastal areas including the 2015 irrigated farm locations have a lower relative sensitivity to RH_{mean}, with a less marked annual cycle than interior areas.

Higher SCs for R_s are apparent (Figure 5) along an interior band that goes from the northwest to the southeast on the island and generally coincides with more humid regions (Figure 2a), consistent with the findings of Tabari and Talaee [36] for Iran and Emeka et al. [18] for Nigeria. ET_o is relatively less sensitive to R_s along the northeast coast and especially along the south coast. Although a clear seasonal cycle of higher relative sensitivity to R_s during the summer months is evident (Figures 5 and 9), its amplitude is much smaller than that of RH_{mean}. Although, overall, the SCs for R_s and T_{max} are quite close on an island-wide basis (0.57 and 0.50, respectively), their spatial and temporal patterns are generally opposite (Figures 5, 6 and 9). ET_o is relatively less sensitive to T_{max} along interior mountainous regions of the island and during the summer months, and more sensitive along coastal areas, especially in the southern and western coasts during the dry season months. Seasonal variations in the relative sensitivity to T_{max} are relatively minor, especially in mountainous areas (cell 45 in Figures 1 and 9). Minimal spatial and temporal variation in the SCs for T_{min} was found, with only slightly lower values in the western interior areas of the island from January to April and slightly higher values in coastal areas to the east (Figure 7).

Many similarities in the spatial and temporal patterns of SCs to u_2 (Figure 8) and the spatial and temporal patterns of SCs to T_{max} (Figure 6) were found. However, ET_o is much less sensitive to relative changes in u_2 than in T_{max} (Figure 9). The relative sensitivity of ET_o to changes in T_{max} and u_2 is lower along humid and warm interior mountainous regions of the island and during the rainy summer months, and higher along coastal areas, especially in the southern coast during the dry season months. These findings are consistent with those of Emeka et al. [18] for Nigeria and Tabari and Talaee [36] for Iran. The lower sensitivity of ET_o to changes in wind speed in humid and warm environments compared to its higher sensitivity in hot and dry environments is explained by Allen et al. [32]. In humid and warm conditions, such as in the interior mountains, the wind (no matter how intense) can only replace saturated air at the vegetation's surface with air from above that is only slightly less saturated, thereby limiting potential increases in evapotranspiration. Increases in wind speed may, in fact, increase sensible heating more than evapotranspiration in these humid and warm environments, resulting in slightly negative SCs for u_2 at times (Figure 8 and cell 16 in Figure 9). In contrast, in hot and dry environments, such as the island's south coast, increases in wind speed can increase the evapotranspiration rate more since the atmosphere is thirstier and has more energy available.

Figure 10 shows the percent change in ET_o due to +/− 5, 10, 15, 20, and 25% changes in basic meteorological variables at selected GOES-PRWEB grid cell locations shown in Figure 1 and the average at the 2015 irrigated farm locations. The larger relative sensitivity of ET_o to changes in RH_{mean} compared to other variables is evident in the larger slope for the RH_{mean} line. Linearity in the SCs is observed over the tested range of percentage changes in the basic meteorological variables at all grid cells, which means that the application of the SC values at the origin over a relatively wide range of changes in the meteorological variables is appropriate.
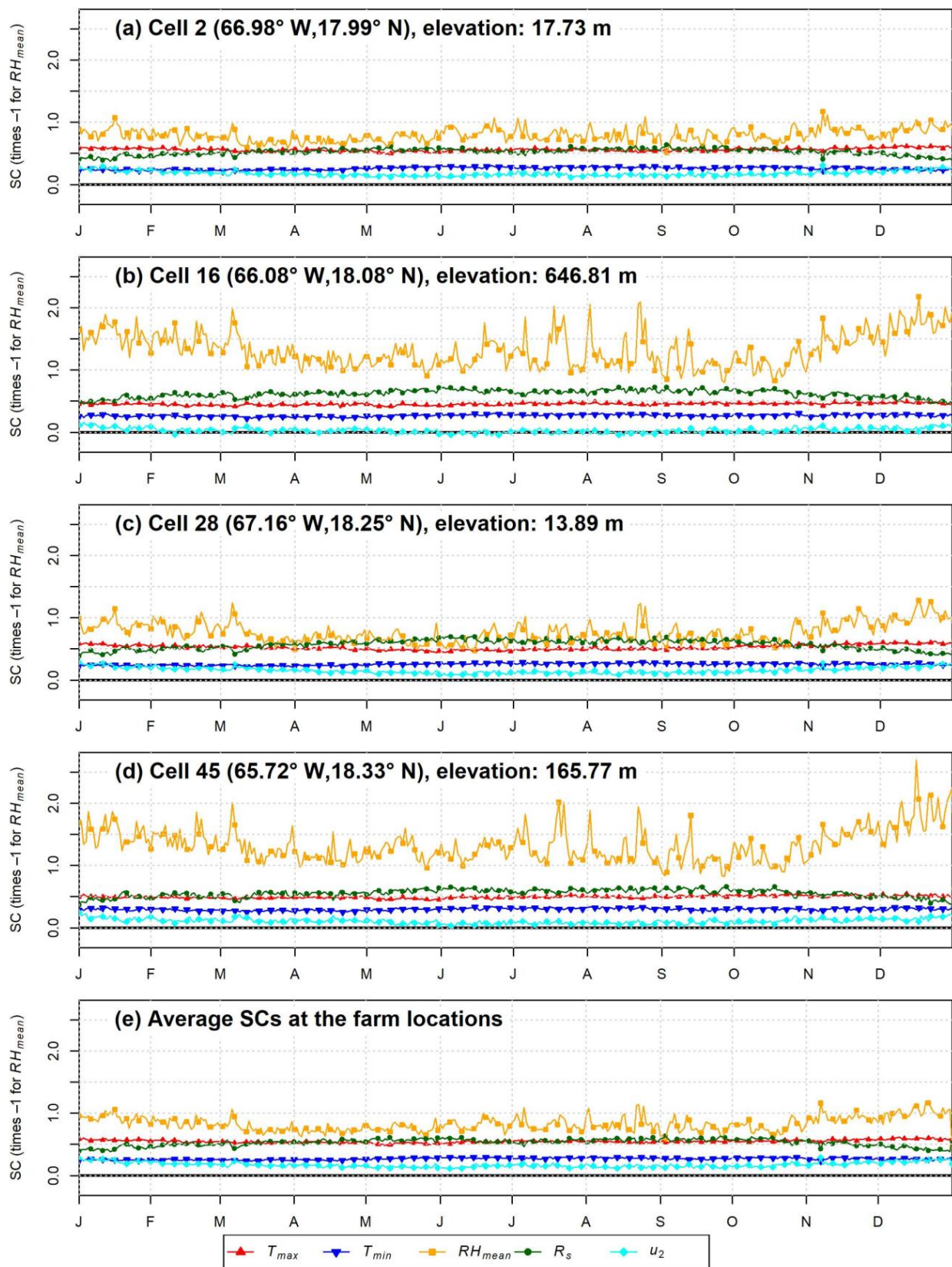
Figure 9. Daily timeseries of sensitivity coefficients (SCs) at: (**a**–**d**) representative GOES-PRWEB grid cell locations (Figure 1) and (**e**) average at grid cells associated with the 2015 irrigated farm locations. Markers are shown every 5 days. Cell 2 is on the southwest coast; cell 16 is located near the Sierra de Cayey; cell 28 is on the west coast; cell 45 is located near the Sierra de Luquillo.
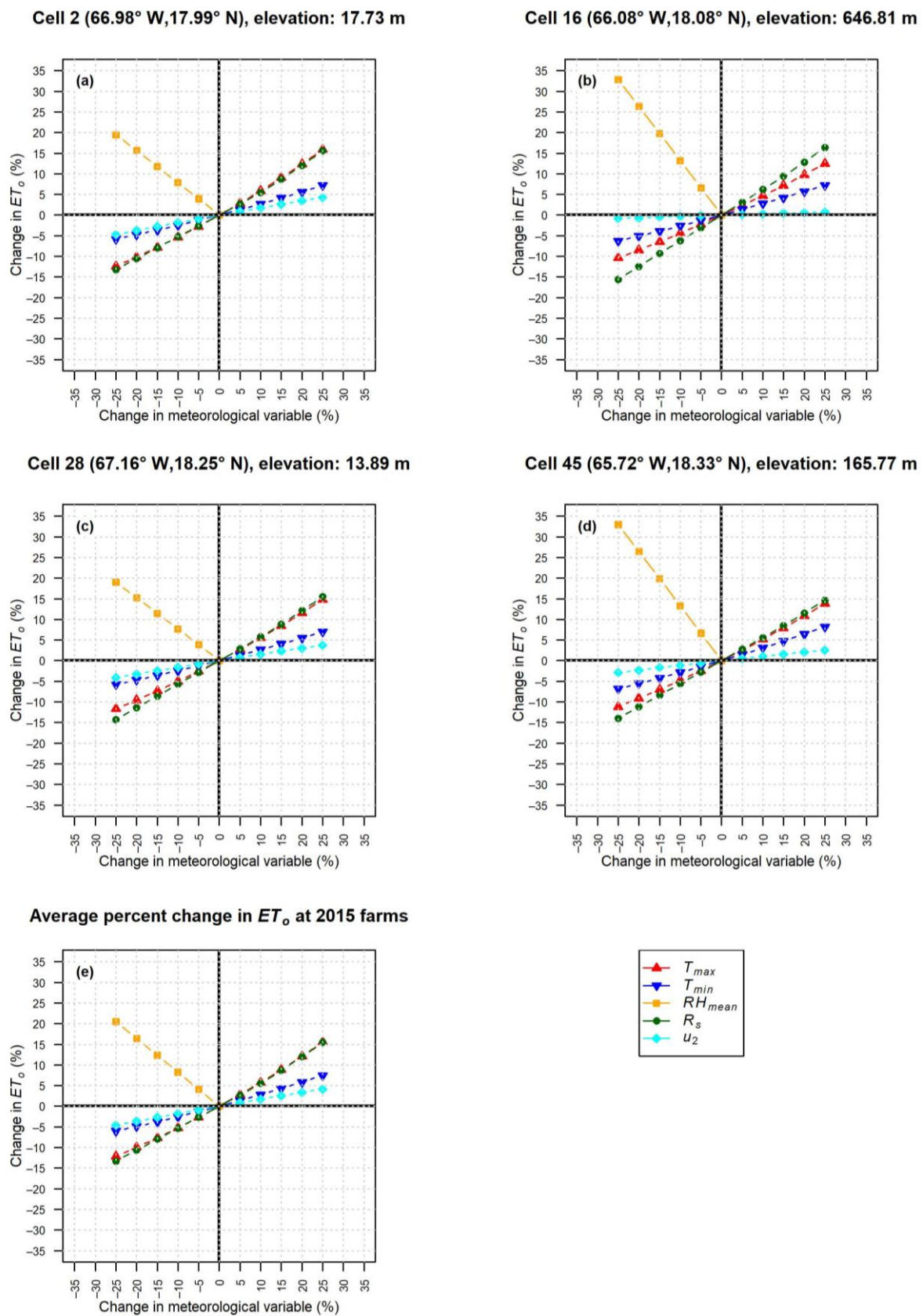
Cell 2 (66.98° W,17.99° N), elevation: 17.73 m

Cell 16 (66.08° W,18.08° N), elevation: 646.81 m

Cell 28 (67.16° W,18.25° N), elevation: 13.89 m

Cell 45 (65.72° W,18.33° N), elevation: 165.77 m

Average percent change in ET_o at 2015 farms

Figure 10. Percentage change in ET_o due to $+/-$ 5, 10, 15, 20, and 25% change in basic meteorological variables at: (**a–d**) representative GOES-PRWEB grid cell locations (Figure 1) and (**e**) average at grid cells associated with the 2015 irrigated farm locations.

The Pearson correlation matrix is presented between long-term monthly maps of basic meteorological variables, their SCs, components of ET_o, rainfall, and elevation (Table 1). The SC for RH_{mean} has not been multiplied by -1 when calculating correlations. To aid in the discussion, Figures S1–S11 show maps of the long-term monthly average for the basic meteorological variables, rainfall, and components of ET_o. The SC for RH_{mean} (Figure 4 shows the SC for RH_{mean} multiplied by -1) is highly anti-correlated to RH_{mean} (Figure S1), specifically to the spatial pattern in RH_{mean}. In other words, ET_o is most sensitive to changes in RH_{mean} in areas where RH_{mean} already tends to be high and limiting, such as in the high-elevation areas of the Cordillera Central and the Sierra de Luquillo, where it exceeds about 82% on average (Figure S1). In these areas, lower R_s (Figure S2) also results in a lower contribution from $ET_{o,energetic}$ (Figure S7). The absolute value of the SC for RH_{mean} is also highest in winter when aerodynamic effects become more important due to lower solar radiation. RH_{mean} is highly anti-correlated to $ET_{o,aerodynamic}$ and $ET_{o,aerodynamic\ fraction}$, as expected, since an increase in RH_{mean} decreases the VPD and reduces these terms. RH_{mean} is also highly correlated to elevation (Figure 1) and highly anti-correlated to T_{max} reflecting the higher RH_{mean} and the lower T_{max} in the interior mountainous areas, and the opposite trends in coastal areas. RH_{mean} is also highly anti-correlated to the SCs for T_{max} and for u_2. This is expected since these three variables act synergistically to increase $ET_{o,aerodynamic}$, especially during winter.

The SC for R_s (Figure 5) is generally higher along the higher-elevation interior areas and moderately correlated to R_s (Figure S2). They are highly correlated in time (i.e., months with lowest R_s are also the months with lowest SC for R_s) but somewhat anti-correlated in space (i.e., areas with the lowest R_s in the interior mountains have the highest SC for R_s). The SC for R_s is moderately correlated to $ET_{o,energetic}$ (Figure S7), especially in time. The sensitivity to R_s is highest from northwest to southeast interior areas, especially in summer when R_s and $ET_{o,energetic}$ are at their highest and tend to dominate over aerodynamic effects (Figures S9 and S10). In winter, the aerodynamic term dominates more, so that R_s is not as important in driving ET_o on the southwest coast for example (Figure 5). As expected, $ET_{o,energetic}$ (Figure S7) is very highly correlated to R_s and to elevation since R_s is moderately anti-correlated to elevation (Figure 1) due to the common presence of clouds at higher elevations. R_s is moderately correlated to T_{max} and T_{min}. This is most evident in the interior mountainous areas where R_s, T_{max}, and T_{min} tend to be the lowest. R_s is moderately correlated to the SC for RH_{mean} (Figure 4) since R_s tends to be higher along coastal areas where the SC for RH_{mean} is higher (less negative).

Rainfall from GOES-PRWEB was only found to be moderately correlated to the SC for R_s and $ET_{o,energetic\ fraction}$. The correlation between rainfall and elevation was found to be quite low at only 0.02. Figure 2a shows two distinct areas of high rainfall—in the Sierra de Luquillo on the eastern side of the island, and in the northwest central part of the island (Figure 1). The spatial variability of rainfall results from easterly to northeasterly winds interacting with the local orography. However, rainfall appears to occur predominantly on the windward side of the mountains and not exactly at the locations with highest elevations. Even in the Sierra de Luquillo, the expectation of higher rainfall at higher elevations may not hold. Based on a relatively large set of rain gauges, Murphy et al. [37] found that the long-held assumption of precipitation increasing consistently with elevation within the Sierra de Luquillo does not hold. They found that leeward (western) watersheds in the mountains generally receive lower mean annual precipitation than windward (eastern) watersheds.

Table 1. Pearson correlation coefficient (r) matrix between long-term monthly maps of basic meteorological variables, their sensitivity coefficients (*SCs*), components of ET_o, rainfall, and elevation. ET_o is the reference evapotranspiration, RH_{mean} is the daily mean relative humidity, R_s is the daily incoming solar radiation, T_{max} is the daily maximum air temperature, T_{min} is the daily minimum air temperature, and u_2 is the 2 m wind speed. ET_o *energ. (frac.)* and ET_o *aero. (frac.)* are the energetic and aerodynamic ET_o components (and their fractions), respectively.

Variable	RH_{mean}	R_s	T_{max}	T_{min}	u_2	SC RH_{mean} *	SC R_s	SC T_{max}	SC T_{min}	SCu_2
RH_{mean}	1	−0.29	−0.72	−0.49	−0.02	−0.73	0.47	−0.69	0.07	−0.80
R_s	−0.29	1	0.54	0.57	0.30	0.56	0.55	−0.07	0.25	−0.26
T_{max}	−0.72	0.54	1	0.88	0	0.76	−0.01	0.67	0.31	0.51
T_{min}	−0.49	0.57	0.88	1	0.22	0.51	0.06	0.49	0.70	0.33
u_2	−0.02	0.30	0	0.22	1	−0.39	−0.25	0.08	0.55	−0.01
SC RH_{mean} *	−0.73	0.56	0.76	0.51	−0.39	1	0.18	0.33	−0.17	0.34
SC R_s	0.47	0.55	−0.01	0.06	−0.25	0.18	1	−0.64	−0.01	−0.83
SC T_{max}	−0.69	−0.07	0.67	0.49	0.08	0.33	−0.64	1	0.20	0.86
SC T_{min}	0.07	0.25	0.31	0.70	0.55	−0.17	−0.01	0.20	1	0.04
SC u_2	−0.80	−0.26	0.51	0.33	−0.01	0.34	−0.83	0.86	0.04	1
ET_o *energ.*	−0.30	0.96	0.65	0.65	0.10	0.66	0.62	−0.05	0.23	−0.23
ET_o *aero.*	−0.86	0.48	0.72	0.67	0.49	0.49	−0.44	0.67	0.31	0.66
ET_o *energ. frac.*	0.68	0.24	−0.30	−0.23	−0.39	−0.04	0.94	−0.77	−0.16	−0.90
ET_o *aero. frac.*	−0.68	−0.24	0.30	0.23	0.39	0.04	−0.94	0.77	0.16	0.90
Rainfall	0.27	0.17	0.17	0.19	−0.32	0.15	0.60	−0.27	0.05	−0.38
Elevation	0.78	−0.65	−0.92	−0.92	−0.10	−0.66	0.68	−0.85	−0.47	−0.84

Variable	ET_o *energ.*	ET_o *aero.*	ET_o *energ. frac.*	ET_o *aero. frac.*	*Rainfall*	*Elevation*
RH_{mean}	−0.30	−0.86	0.68	−0.68	0.27	0.78
R_s	0.96	0.48	0.24	−0.24	0.17	−0.65
T_{max}	0.65	0.72	−0.30	0.30	0.17	−0.92
T_{min}	0.65	0.67	−0.23	0.23	0.19	−0.92
u_2	0.10	0.49	−0.39	0.39	−0.32	−0.10
SC RH_{mean} *	0.66	0.49	−0.04	0.04	0.15	−0.66
SC R_s	0.62	−0.44	0.94	−0.94	0.60	0.68
SC T_{max}	−0.05	0.67	−0.77	0.77	−0.27	−0.85
SC T_{min}	0.23	0.31	−0.16	0.16	0.05	−0.47
SC u_2	−0.23	0.66	−0.90	0.90	−0.38	−0.84
ET_o *energ.*	1	0.42	0.32	−0.32	0.33	−0.88
ET_o *aero.*	0.42	1	−0.72	0.72	−0.32	−0.80
ET_o *energ. frac.*	0.32	−0.72	1	−1	0.56	0.77
ET_o *aero. frac.*	−0.32	0.72	−1	1	−0.56	−0.77
Rainfall	0.33	−0.32	0.56	−0.56	1	0.02
Elevation	−0.88	−0.80	0.77	−0.77	0.02	1

* The SC for RH_{mean} has not been multiplied by −1 when calculating correlations.

The SC for T_{max} (Figure 6) is higher along the low-elevation coastal areas, especially along the south coast, and it is moderately correlated to T_{max} (Figure S3). They are highly correlated spatially; however, they appear anti-correlated in time. That is, the cooler winter

months with lower T_{max} show a higher sensitivity to T_{max} as the energetic term decreases and the aerodynamic term's importance increases, especially along the southwest coast (Figures S9 and S10). T_{max} (Figure S3), T_{min} (Figure S4), and elevation (Figure 1) are very highly correlated due to lower temperatures in the interior mountain regions. T_{max} stays relatively high in the southwest coast year-long, whereas T_{min} is reduced during winter and early spring in the area, resulting in a higher daily temperature range in the area in winter and early spring. T_{max} is moderately to highly correlated to both $ET_{o,energetic}$ (Figure S7) and $ET_{o,aerodynamic}$ (Figure S8) because it affects both terms; however, it appears to affect ET_o and especially the aerodynamic component more in the winter when it acts synergistically with u_2 and RH_{mean} to increase it, especially along coastal areas. T_{max} is also highly correlated to the SCs for RH_{mean} (Figure 4) and has a moderate correlation to the SC for u_2 (Figure 8). This is expected since these three variables act synergistically to increase $ET_{o,aerodynamic}$, especially during winter. The SC for T_{min} (Figure 7) is highly correlated to T_{min} (Figure S4). The correlation is stronger in time than in space. T_{min} is moderately correlated to both $ET_{o,energetic}$ (Figure S7) and $ET_{o,aerodynamic}$ (Figure S8) since it affects both terms.

The SC for u_2 (Figure 8) is generally higher along coastal areas and has no correlation to the spatial pattern in u_2 (Figure S5). As expected, u_2 is moderately correlated to $ET_{o,aerodynamic}$ (Figure S8); u_2 is also moderately correlated to the sensitivity coefficient for T_{min} (Figure 7). The SCs for R_s (Figure 5) and for T_{max} (Figure 6) are moderately anti-correlated. This is especially true in time (i.e., in winter months, the SC for R_s decreases while the SC for T_{max} increases, especially in coastal areas), but also to a lesser extent in space (i.e., interior areas have the highest SCs for R_s and the lowest SC for T_{max}). The SCs for R_s (Figure 5) and for u_2 (Figure 8) are highly anti-correlated. This is especially true in time (i.e., in winter months, the SC for R_s decreases while the SC for u_2 increases, especially in coastal areas), but also to a lesser extent in space (i.e., interior areas have the highest SCs for R_s and the lowest SC for u_2). The SCs for T_{max} (Figure 6) and for u_2 are highly correlated in both space and time. The SC for RH_{mean} (Figure 4) is moderately correlated to $ET_{o,energetic}$ (Figure S7) and has a moderate correlation to $ET_{o,aerodynamic}$ (Figure S8). The SC for R_s (Figure 5) is moderately correlated to $ET_{o,energetic}$ (Figure S7) and very highly correlated to $ET_{o,energetic\ fraction}$ (Figure S9), as expected.

3.3. Application

Timeseries of SCs are presented by day of the year (Figure 9e) at the GOES-PRWEB grid cells at the 2015 irrigated farms, most of which are located along the south coast (Figure 1). Compared to interior areas, the areas including the 2015 irrigated farm locations show a lower relative sensitivity to RH_{mean} (Figure 4) with a less marked annual cycle. ET_o is also relatively less sensitive to R_s (Figure 5) in these areas, especially during winter months when ET_o becomes more sensitive to relative changes in T_{max} (Figure 6). The relative sensitivity of ET_o to changes in u_2 is lower than for other variables but higher along the southern coast than in other areas, especially during the dry season. In hot and dry environments, such as the south coast, increases in wind speed can increase the evapotranspiration rate more since the atmosphere has a lower moisture content and more energy available.

The lowest $ET_{o,energetic\ fraction}$ (Figure S9) and the highest $ET_{o,aerodynamic\ fraction}$ (Figure S10) occur in the south coast of Puerto Rico. This is due to this region having the highest T_{max} (Figure S3) and the lowest RH_{mean} (Figure S1) (which results in a high VPD) combined with moderate wind speeds in this area (Figure S5). These factors result in comparatively high $ET_{o,aerodynamic}$ (Figure S8) and $ET_{o,aerodynamic\ fraction}$ (Figure S10) compared to other areas. The low RH_{mean} and relatively low cloudiness on the south coast also traps less longwave radiation in the atmosphere, reducing the net radiation, which would tend to reduce the energetic term. However, this effect appears to be counteracted by higher R_s (Figure S2) due to the lower cloudiness for a net result of higher incoming net radiation and higher $ET_{o,energetic}$ (Figure S7) compared to other areas.

3.3.1. Causes of Errors in Reference ET Estimated from Model Output for 1985–2005

Combining the average SCs at the 2015 irrigated farm locations on a monthly basis (Figure 11a) with the percent error in the simulated basic meteorological variables for the period 1985–2005 with respect to GOES-PRWEB for 2009–2017 according to Equation (3) gives the total contribution of each variable to errors in estimated ET_o for the two down-scaled GCMs (Figure 11b,c). The individual lines in these plots show the product of the SC for a particular basic meteorological variable times the percent error in the variable, which gives the contribution of that variable to the total error in ET_o as a percentage. The brown line shows the total computed error in ET_o ($\frac{dET_o}{ET_o}$ in Equation (3), as a percentage), and the black line shows the sum of the contributions from all the five basic meteorological variables to the total error in ET_o ($\sum_i \left(\frac{\partial ET_o}{\partial V_i} \times \frac{V_i}{ET_o} \times \frac{dV_i}{V_i} \right)$ in Equation (3)). The difference between the black and brown lines is the approximation error (*error* in Equation (3)). The individual error components add up to large negative monthly biases in ET_o of up to −21.1% for CNRM and −12.3% annually. The largest and most consistent contributors to those negative biases appear to be the well-documented [9] cold model biases for both T_{max} and T_{min}. However, biases in all five meteorological variables act synergistically to result in a large underestimation of ET_o during October–December in CNRM. Despite ET_o being most sensitive to relative errors in RH_{mean} than in the other variables, smaller relative biases in RH_{mean} in CNRM compared to other variables resulted in a smaller contribution of RH_{mean} to errors in ET_o.

In CESM, the cold biases for T_{max} and T_{min} are compensated by positive contributions to ET_o bias from other meteorological variables during certain parts of the year, resulting in overall lower annual bias (−0.5%) than CNRM, and monthly biases ranging from −9.8% to 7.2%. Therefore, only bias correcting model output for precipitation and temperature, as is commonly done due to the widespread availability of observational gridded datasets for these two variables, is not always appropriate. Here, it would decrease the biases in ET_o for CNRM but increase them for CESM. Although the existence of a cold bias in the downscaled models has been identified in other studies, it is important to note that some of the apparent errors in the other variables may be due to the different periods being compared between the model historical simulation and the observations.

3.3.2. Causes of Changes in Reference ET Estimated from Model Output for 2040–2060

The monthly SCs at the 2015 irrigated farm locations (Figure 11a) were also combined with the percent change in the simulated basic meteorological variables from 1985–2005 to 2040–2060 to obtain the total contribution of each variable to projected changes in ET_o for the two downscaled GCMs (Figure 11d,e). The individual lines in these plots show the product of the SC for a meteorological variable times the percent change in the variable from 1985–2005 to 2040–2060, which gives the contribution of that variable to the total change in ET_o as a percentage. The brown line shows the total computed change in ET_o ($\frac{dET_o}{ET_o}$ in Equation (3), as a percentage), and the black line shows the sum of the contributions from all five basic meteorological variables to the total change in ET_o ($\sum_i \left(\frac{\partial ET_o}{\partial V_i} \times \frac{V_i}{ET_o} \times \frac{dV_i}{V_i} \right)$ in Equation (3)). The difference between the black and brown lines is the approximation error (*error* in Equation (3)). Both models project an overall 5.6% increase in annual ET_o mainly due to projected increases in T_{max} and T_{min} and a decrease in RH_{mean}; however, the seasonality of the changes is different between the two models, as shown in Figure 11d,e. The projected decline in RH_{mean} indicates a sub-Clausius–Clapeyron relationship (i.e., humidity increasing at rates lower than the 7% predicted by the Clausius–Clapeyron relationship; [38]) for the region which, together with the projected reductions in rainfall, may be a result of decreased moisture convergence into the region during the period 2040–2060. Despite ET_o being most sensitive to relative changes in RH_{mean} than in the other variables, smaller relative changes in RH_{mean} in both models compared to T_{max} and T_{min}, result in similar contributions to changes in ET_o from the three variables. The contribution of increases in u_2 to increases in ET_o is also positive but minor. CNRM

shows small changes in R_s during most months, while CESM shows a small decrease in R_s during most of the year. CESM projects larger increases in ET_0 during March, November, and December, increasing the potential for crop water stress during those times.
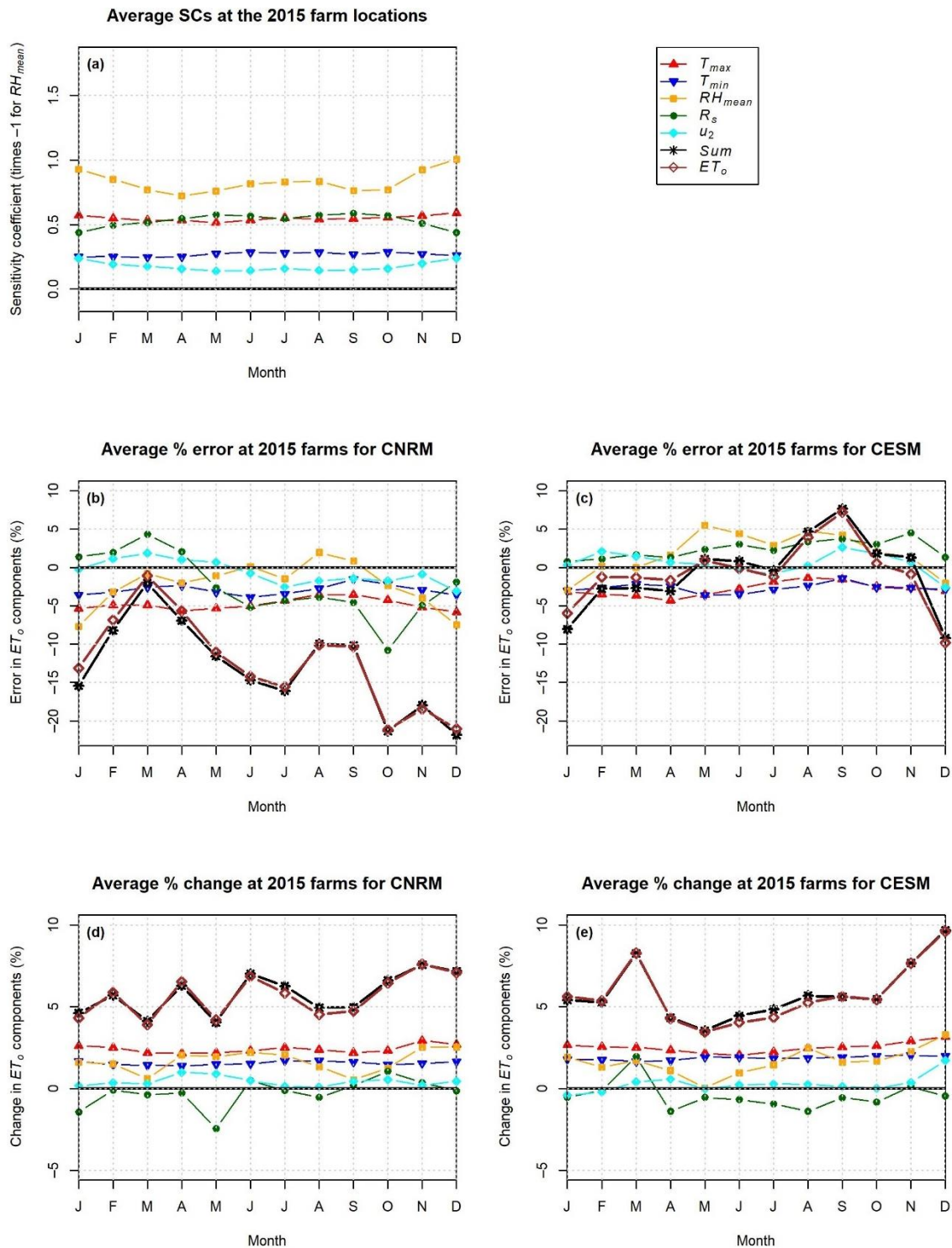

Figure 11. (**a**) Timeseries of SCs at the 2015 irrigated farm locations. (**b,c**) Average percent error in ET_0 estimated for the period 1985–2005, contributions from the basic meteorological variables, and their sum for CNRM and CESM, respectively. (**d,e**) Average percent change in ET_0 from 1985–2005 to 2040–2060, contributions from the basic meteorological variables, and their sum for CNRM and CESM, respectively.

3.4. Limitations

Some key factors that were not considered in the application of the derived SCs to understanding potential future changes in ET_o (and ET_c) include increases in stomatal resistance and increases in photosynthesis in C3 plants and in C4 plants under drought [39] due to projected increases in atmospheric CO_2 concentrations (CO_2). These changes in plant physiology may counteract some of the expected increases in ET_c from increased evaporative demand (ET_o) due to higher temperatures [40]. Changes in stomatal resistance due to increases in CO_2 can be informed by free-air carbon dioxide enrichment (FACE) experiments [39] and could be applied as modifications to the crop potential transpiration term to obtain estimates of ET_c under future conditions, as in Kruijt et al. [41] and Scarpare et al. [42]. However, crop growth models are needed to better understand potential future changes in ET due to changes in plant biomass from increased photosynthesis and other factors, such as changes in stomatal resistance due to meteorological changes and changes in soil moisture, changes in planting dates and speed of plant growth, and feedbacks between these factors. For example, Scarpare et al. [42] used the CropSyst model to investigate potential future changes in ET_c for five major irrigated crops in the Columbia Basin for 15 bias-corrected and statistically downscaled GCMs under the CMIP5 RCP8.5 scenario. Full irrigation was assumed to avoid crop water stress. For the 2090s, they found that changes in ET_c ranged from −12.5% to +14.3% depending on the crop and the interplay of different meteorological, crop, and management factors. The application of a crop growth model to estimate changes in ET_c for the main crops in Puerto Rico would help clarify potential future changes in agricultural irrigation requirements and aid water management planning efforts.

Additional sources of uncertainty include the effect of neglecting changes in soil heat flux density at the soil surface and changes in water heat flux density over areas with ponding water, which may be important during advective conditions such as cold fronts. In addition, there is an assumption that GOES-PRWEB meteorological and ET_o data are reasonably accurate compared to observations, which may not necessarily be the case given that some of the data are derived from climate models, as described in Harmsen et al. [28]. As previously mentioned, the GOES-PRWEB estimated ET_o, and its driving meteorological variables have been validated by Mecikalski and Harmsen [29] and Harmsen et al. [28,30] at a few stations on the island. The GOES-PRWEB precipitation and T_{max} and T_{min} fields have also been validated at stations throughout the island. However, efforts to validate the GOES-PRWEB dataset in a more comprehensive manner have been limited in particular by the lack of homogeneous, high-quality humidity, solar radiation, and wind speed data at a large number of stations on the island. For solar radiation in particular, some of the existing station data can show sensor issues, such as change points and drifts. In addition, at stations along the interior of the island, the upper envelope of daily solar radiation values is often well below a reasonable clear-sky radiation curve for the time of year, indicating that the station may be shaded by the local canopy or nearby obstructions (buildings, topographic features) for the majority of the year.

Similar concerns occur for wind speed data and are exacerbated by the lack of documented (changes in) sensor heights at meteorological stations. The sensitivity of ET_o to changes in RH_{mean} has been found to increase with increasing wind speed [12]. This is consistent with our finding of moderate autocorrelation between SC for RH_{mean} and u_2 (r of −0.39 in Table 1) which means that as u_2 increases, the SC for RH_{mean} becomes more negative (i.e., the absolute of the SC for RH_{mean} increases). Therefore, errors in u_2 from GOES-PRWEB may affect the relative ranking of SCs across meteorological variables. In particular, an overestimation of u_2 in GOES-PRWEB would result in an overestimation of the SC for RH_{mean}, which was found to be the meteorological variable with the highest relative sensitivity. For this reason, in Appendix S5, wind-speed records at stations throughout the island were compared with GOES-PRWEB wind speeds at the grid cell closest to each station (Table S1 and Figure S12). When sensor height information is available at a station (Table S1), it was used to convert the wind speeds to 2 m heights using the relationship

in [10] for consistency with u_2 from GOES-PRWEB. Generally, wind sensors are installed at meteorological stations at 2 to 10 m heights, for which conversion factors to 2 m (based on [10]) range from 1 to 0.75, respectively. Therefore, when sensor height information is not available, a discrepancy of up to about 25% between station wind speeds and u_2 from GOES-PRWEB can be expected on average.

Figure S12b shows that the percent difference between GOES-PRWEB u_2 and sensor wind speed (converted to 2 m when possible) ranges between -23% and 225%. Notably, 16 out of 22 stations have percent differences between $+/-$ 35%, which appear reasonable. However, high percent differences are observed at some stations along the southwest and southeast coasts and along the interior of the island. Furthermore, some of these stations with the higher percent differences are relatively close to other stations with lower percent differences, such as at the Yabucoa stations for example. These large discrepancies in percent differences within short distances may be due to various reasons, including incorrect measurement units, coordinates, or sensor height reported for the station, station sheltering, comparison of 1 km wind speeds from GOES-PRWEB versus point values, and large gradients occurring within small areas. The Global Wind Atlas [43] is a web-based application that provides estimates of wind speed for wind power generation worldwide. It uses the WRF model to downscale reanalysis data in the ERA5 dataset from the European Centre for Medium-Range Forecasts (ECMWF; [44]). The resulting 3 km wind speeds are then generalized and applied to a microscale modeling system to determine local wind climates at 250 m resolution at heights ranging from 10 to 200 m. The microscale model considers orography, roughness and roughness-change effects, including speed-up effects as the wind moves up a mountain or hill. The Global Wind Atlas shows a large gradient in the annual average 10 m wind speed from coastal to offshore areas of Puerto Rico and high variability in wind speeds over mountainous areas resulting from changes in roughness and orography. The 1 km GOES-PRWEB dataset is not expected to capture these localized changes. This likely explains the large changes in wind speed performance over small distances and the overestimation of wind speeds in GOES-PRWEB at interior stations.

Due to the uncertainty in wind speeds and the potential for its overestimation in GOES-PRWEB at some station locations, a sensitivity analysis was performed on the SCs where GOES-PRWEB u_2 was multiplied by factors equal to 0.67 and 0.5 to counteract possible overestimation of wind speeds in GOES-PRWEB by 50% and 100%, respectively. This sensitivity analysis represents the worst-case scenario, where it is assumed that the GOES-PRWEB u_2 is overestimated island wide, when Figure S12 shows that is clearly not the case. Results from this sensitivity analysis are shown in Appendix S5, where Figure 9 is recreated for the two factors (Figures S13 and S14; Table S2). As the wind speed is reduced, the SC for RH_{mean} decreases and the SC for R_s increases. At some locations, such as cells 16 and 45 (Figure 1), the SC for RH_{mean} remains mostly larger than the SC for R_s throughout the year when 0.67 u_2 is used (Figure S13), but only in the winter months when 0.5 u_2 is used (Figure S14). In the case when 0.67 u_2 is used, the SC for RH_{mean} becomes comparable to the SC for R_s at many locations throughout the island, whereas when 0.5 u_2 is used, it becomes smaller than the SC for R_s, as reflected in the island-wide average SCs (Table S2).

As observed in Figure 3c, it was also found that the standard deviation of annual ET_o at the location of 2015 irrigated farms and golf courses is much higher for GOES-PRWEB (97.0 mm/year for 2009–2017) than for the two downscaled climate models (35.7 and 35.6 mm/year for CESM, and CNRM, respectively, in the period 1985–2005) and the Herrera-Ault dataset (24.6 mm/year for 1985–2005). The larger interannual variability in GOES-PRWEB ET_o may be due to the switch of datasets used in its derivation, as described by Harmsen et al. [28]. As previously discussed, the annual cycle of station-based estimates of ET_o appears to match that of GOES-PRWEB better than that of Herrera-Ault (Figure 3b), with peak values in July as in GOES-PRWEB rather than in March as in Herrera-Ault. Since the exact magnitude of interannual variability of ET_o in the study area is unknown, and the downscaled climate models show interannual variability within the range of the two obser-

vational datasets, it may be sensible to bias correct model-based ET_o using GOES-PRWEB on monthly timescales only (i.e., no corrections for interannual variability).

4. Discussion

It was found that the SC for RH_{mean} dominates the sensitivity of ET_o throughout most of the island, even more so than the SCs for R_s and T_{max}. This is because the high relative humidity over most of the island currently limits ET_o and there is plenty of energy (R_s and T_{max}) available for ET_o in most areas during most of the year. The SC for RH_{mean} has a large-amplitude annual cycle, especially along the Cordillera Central mountains and the Sierra de Luquillo with larger values and less day-to-day variability in the dry season than in the wet season. Coastal areas, including the 2015 irrigated farm locations, show a lower relative sensitivity to RH_{mean}, with a less marked annual cycle than interior areas. The overall ranking of sensitivities found in our study (SC for RH_{mean} > SC for R_s > SC for T_{max} > SC for T_{min} > SC for u_2) is similar to that obtained for the tropical rainforest climate of southern Nigeria [18] and for the Yangtze River Basin in China [12]. However, the SCs are not very meaningful on their own unless combined with a measure of the variability measurement/estimation error or changes in the basic meteorological variables with time.

Our main objective in deriving SCs for Puerto Rico was to guide the prioritization of bias correction of meteorological output for ET_o estimation from dynamically downscaled climate projections, which can then be used to drive a soil-moisture water-balance model [2] for estimating future agricultural irrigation requirements on the island. This objective was met by applying the SCs to understand the sources of error and potential future changes in ET_o estimated from downscaled model output at the 2015 irrigated farm locations. The results illustrate how the ranking of variable importance may change when the SCs are combined with estimates of error or change in meteorological variables. For example, despite ET_o being most sensitive to relative errors in RH_{mean}, relative biases in RH_{mean} in the CNRM model are small compared to other variables. This results in a smaller contribution of RH_{mean} to errors in CNRM-estimated ET_o. Similarly, despite ET_o being most sensitive to relative changes in RH_{mean} than in the other variables, smaller relative future changes in RH_{mean} compared to T_{max} and T_{min} in both climate models result in similar contributions to future changes in ET_o from the three variables.

For the period 2040–2060, it was found that both climate models project an overall 5.6% increase in annual ET_o over the 2015 irrigated farm locations with respect to the historical period 1985–2005. This increase in ET_o is primarily a result of projected increases in T_{max} and T_{min} and a decrease in RH_{mean}, with differences in the seasonality of changes between the two models. Absent compensatory increases in rainfall and/or a compensatory decrease in ET_o due to stomatal closure as CO_2 increases, the future increase in ET_c resulting from the 5.6% increase in ET_o may have to be met by an additional volume of irrigation. Future research could attempt to estimate the additional agricultural irrigation requirements and their sensitivity to various bias-correction choices.

Various limitations of the current study are highlighted in the results. They include uncertainties in the stomatal and plant-growth responses to projected increases in atmospheric CO_2, uncertainties in crop suitability under climate change, the effect of neglecting changes in soil and water heat fluxes in the ET_o equation, and the lack of sufficient meteorological data at weather stations to corroborate meteorological data and ET_o estimates and the derived sensitivity coefficients. The development of reliable homogeneous spatially distributed long-term observational datasets of meteorological and hydrological variables is imperative for improving the understanding of drivers of hydrological processes, evaluating model performance, and for bias correction of model output.

References

1. Puerto Rico Institute of Statistics. Food Security in Puerto Rico, Calendar Year 2015. 2019. Available online: https://estadisticas.pr/files/Comunicados/Seguridad%20Alimentaria%20en%20Puerto%20Rico%20-%20Final%20%28300519%29.pdf (accessed on 20 July 2022).
2. Molina-Rivera, W.L.; Irizarry-Ortiz, M.M. Estimated water withdrawals and use in Puerto Rico. *U.S. Geol. Surv. Open-File Rep.* **2021**, *2021–1060*, 1–38.
3. Puerto Rico Planning Board. Memorial of the Land Use Plan, Guide for the Classification of Territories. 2015. Available online: https://www.sciencebase.gov/catalog/item/576bfe89e4b07657d1a26ee5 (accessed on 8 February 2023).
4. Puerto Rico Department of Natural and Environmental Resources. Integrated Water Resources Plan for Puerto Rico. 2016. Available online: https://drna.pr.gov/wp-content/uploads/formidable/PIRA-2016.pdf (accessed on 8 February 2023).
5. Harmsen, E.W.; Howard-Harmsen, R. Agricultural Water Management and Puerto Rico's Food Insecurity. *Ethos Gubernamental*. Special Edition. September 2019. Available online: https://academic.uprm.edu/hdc/HarmsenPapers/Harmsen_and_Harmsen_Ethos.pdf (accessed on 18 July 2022).

6. NOAA (National Oceanographic and Atmospheric Administration). National Integrated Drought Information System. Available online: https://www.drought.gov/states/puerto-rico (accessed on 20 July 2022).

7. Herrera, D.A.; Ault, T.R.; Fasullo, J.T.; Coats, S.J.; Carrillo, C.M.; Cook, B.I.; Park Williams, A. Exacerbation of the 2013–2016 pan-Caribbean drought by anthropogenic warming. *J. Geophys. Res.* **2018**, *45*, 10619–10626. [CrossRef] [PubMed]

8. Khalyani, A.H.; Gould, W.A.; Harmsen, E.; Terando, A.; Quinones, M.; Collazo, J.A. Climate change implications for tropical islands: Interpolating and interpreting statistically downscaled GCM projections for management and planning. *J. Appl. Meteorol. Climatol.* **2016**, *55*, 265–282. [CrossRef]

9. Bowden, J.; Terando, A.J.; Misra, V.; Wootten, A.; Bhardwaj, A.; Boyles, R.; Gould, W.; Collazo, J.A.; Spero, T.L. High-resolution dynamically downscaled rainfall and temperature projections for ecological life zones within Puerto Rico and for the U.S. Virgin Islands. *Int. J. Climatol.* **2021**, *41*, 1305–1327. [CrossRef]

10. ASCE (American Society of Civil Engineers); EWRI (Environmental and Water Resources Institute). Task Committee on Standardization of Reference Evapotranspiration. The ASCE Standardized Reference Evapotranspiration Equation. 2005. Available online: https://ascelibrary.org/doi/book/10.1061/9780784408056 (accessed on 20 April 2023).

11. Irmak, S.; Payero, J.O.; Martin, D.L.; Irmak, A.; Howell, T.A. Sensitivity analyses and sensitivity coefficients of standardized daily ASCE Penman–Monteith equation. *J. Irrig. Drain Eng.* **2006**, *132*, 564–578. [CrossRef]

12. Gong, L.; Xu, C.-y.; Chen, D.; Halldin, S.; Chen, Y.D. Sensitivity of the Penman–Monteith reference evapotranspiration to key climatic variables in the Changjiang (Yangtze River) basin. *J. Hydrol.* **2006**, *329*, 620–629. [CrossRef]

13. McKenney, M.S.; Rosenberg, N.J. Sensitivity of some potential evapotranspiration estimation methods to climate change. *Agric. For. Meteorol.* **1993**, *64*, 81–110. [CrossRef]

14. Debnath, S.; Adamala, S.; Raghuwanshi, N.S. Sensitivity analysis of FAO-56 Penman–Monteith method for different agro-ecological regions of India. *Environ. Process.* **2015**, *2*, 689–704. [CrossRef]

15. Cao, L.; Zhang, Y.; Shi, Y. Climate change effect on hydrological processes over the Yangtze River basin. *Quat. Int.* **2011**, *244*, 202–210. [CrossRef]

16. Liu, Q.; Yang, Z.; Cui, B.; Sun, T. The temporal trends of reference evapotranspiration and its sensitivity to key meteorological variables in the Yellow River Basin, China. *Hydrol. Process.* **2010**, *24*, 2171–2181. [CrossRef]

17. Biazar, S.M.; Dinpashoh, Y.; Singh, V.P. Sensitivity analysis of the reference crop evapotranspiration in a humid region. *Environ. Sci. Pollut. Res.* **2019**, *26*, 32517–32544. [CrossRef] [PubMed]

18. Emeka, N.; Ikenna, O.; Okechukwu, M.; Chinenye, A.; Emmanuel, E. Sensitivity of FAO Penman–Monteith reference evapotranspiration (ETo) to climatic variables under different climate types in Nigeria. *J. Water Clim. Chang.* **2021**, *12*, 858–878. [CrossRef]

19. Hou, L.-g.; Zou, S.-b.; Xiao, H.-l.; Yang, Y.-g. Sensitivity of the reference evapotranspiration to key climatic variables during the growing season in the Ejina oasis northwest China. *SpringerPlus* **2013**, *2* (Suppl. S1), S4. [CrossRef]

20. Luo, Y.; Gao, P.; Mu, X. Influence of meteorological factors on potential evapotranspiration in Yanhe River Basin, China. *Water* **2021**, *13*, 1222. [CrossRef]

21. Wang, T.; Zhang, J.; Sun, F.; Liu, W. Pan evaporation paradox and evaporative demand from the past to the future over China: A review. *WIREs Water* **2017**, *4*, e1207. [CrossRef]

22. Peterson, T.; Golubev, V.S.; Groisman, P.Y. Evaporation losing its strength. *Nature* **1995**, *377*, 687–688. [CrossRef]

23. Roderick, M.L.; Rotstayn, L.D.; Farquhar, G.D.; Hobbins, M.T. On the attribution of changing pan evaporation. *Geophys. Res. Lett.* **2007**, *34*, 251–270. [CrossRef]

24. USGS (U.S. Geological Survey). Climate of Puerto Rico. 2016. Available online: https://www.usgs.gov/centers/caribbean-florida-water-science-center-%28cfwsc%29/science/climate-puerto-rico (accessed on 20 July 2022).

25. Angeles, M.E.; González, J.E.; Ramírez-Beltrán, N.D.; Tepley, C.A.; Comarazamy, D.E. Origins of the Caribbean rainfall bimodal behavior. *J. Geophys. Res.* **2010**, *115*, D11106. [CrossRef]

26. Muñoz, M.M.; Lugo, W.I.; Santiago, C.; Matos, M.; Ríos, S.; Lugo, J. Taxonomic Classification of the Soils of Puerto Rico, 2017. University of Puerto Rico, Mayagüez Campus, College of Agricultural Sciences, Agricultural Experiment Station Bulletin 313. January 2018. Available online: https://www.uprm.edu/tamuk/wp-content/uploads/sites/299/2019/06/Taxonomic_classification_soils_PR_2018_reduced.pdf (accessed on 20 July 2022).

27. Dixon, J.F.; Molina-Rivera, W.L.; Irizarry-Ortiz, M.M.; Christesson, K.R. Spatial and Tabular Datasets of Water Withdrawals and Use in Puerto Rico, 2015. U.S. Geological Survey Data Release 2021. Available online: https://www.sciencebase.gov/catalog/item/600aec34d34e162231fb26d9 (accessed on 9 August 2022).

28. Harmsen, E.W.; Mecikalski, J.R.; Reventos, V.J.; Alvarez Perez, E.; Uwakweh, S.S.; Adorno Garcia, C. Water and energy balance model GOES-PRWEB: Development and Validation. *Hydrology* **2021**, *8*, 113. [CrossRef]

29. Mecikalski, J.R.; Harmsen, E.W. The use of visible geostationary operational meteorological satellite imagery in mapping the water balance over Puerto Rico for water resource management. In *Satellite Information Classification and Interpretation*; Rustamov, R.B., Ed.; IntechOpen: London, UK, 2019.

30. Harmsen, E.W.; Tosado Cruz, P.; Mecikalski, J.R. Calibration of selected pyranometers and satellite derived solar radiation in Puerto Rico. *Int. J. Renew. Energy Technol.* **2014**, *5*, 43–54. [CrossRef]

31. Herrera, D.; Ault, T. Insights from a new high-resolution drought Atlas for the Caribbean spanning 1950–2016. *J. Clim.* **2017**, *30*, 7801–7825. [CrossRef]

32. Allen, R.G.; Pereira, L.S.; Raes, D.; Smith, M. Crop evapotranspiration: Guidelines for computing crop water requirements. *FAO Irrig. Drain. Paper* **1998**, *56*. Available online: https://www.fao.org/3/x0490e/x0490e00.htm (accessed on 18 July 2022).
33. Bowden, J.; Wootten, A.; Terando, A.; Boyles, R. Weather Research and Forecasting (WRF): Puerto Rico and US Virgin Islands Dynamical Downscaled Climate Change Projections. U.S. Geological Survey Data Release 2018. Available online: https://www.sciencebase.gov/catalog/item/5977b95de4b0ec1a4888e493 (accessed on 23 March 2021).
34. McCuen, R.H. A sensitivity and error analysis of procedures for estimating evaporation. *Water Resour. Bull.* **1974**, *10*, 486–498. [CrossRef]
35. Harmsen, E.W.; Goyal, M.R.; Torres-Justiniano, S. Estimating evapotranspiration in Puerto Rico. *J. Agric. Univ. Puerto Rico* **2002**, *86*, 35–54. [CrossRef]
36. Tabari, H.; Talaee, P.H. Sensitivity of evapotranspiration to climatic change in different climates. *Glob. Planet. Chang.* **2014**, *115*, 16–23. [CrossRef]
37. Murphy, S.; Stallard, R.F.; Scholl, M.A.; González, G.; Torres-Sánchez, A.J. Reassessing rainfall in the Luquillo Mountains, Puerto Rico: Local and global ecohydrological implications. *PLoS ONE* **2017**, *12*, e0180987. [CrossRef] [PubMed]
38. Koutsoyiannis, D. Revisiting the global hydrological cycle: Is it intensifying? *Hydrol. Earth Syst. Sci.* **2020**, *24*, 3899–3932. [CrossRef]
39. Ainsworth, E.A.; Long, S.P. 30 years of free-air carbon dioxide enrichment (FACE): What have we learned about future crop productivity and its potential for adaptation? *Glob. Chang. Biol.* **2020**, *27*, 27–49. [CrossRef]
40. Islam, A.; Ahuja, L.R.; Garcia, L.A.; Ma, L.; Sassendran, A.S. Modeling the effect of elevated CO_2 and climate change on reference evapotranspiration in the semi-arid Central Great Plains. *Trans. ASABE* **2012**, *55*, 2135–2146. [CrossRef]
41. Kruijt, B.; Witte, J.-P.M.; Jacobs, C.; Kroon, T. Effects of rising atmospheric CO_2 on evapotranspiration and soil moisture: A practical approach for the Netherlands. *J. Hydrol.* **2008**, *349*, 257–267. [CrossRef]
42. Scarpare, F.V.; Rajagopalan, K.; Liu, M.; Nelson, R.L.; Stöckel, C.O. Evapotranspiration of irrigated crops under warming and elevated atmospheric CO_2: What is the direction of change? *Atmosphere* **2022**, *13*, 163. [CrossRef]
43. Global Wind Atlas Version 3.0. Available online: https://globalwindatlas.info/en/area/Puerto%20Rico/ (accessed on 30 January 2023).
44. Hersbach, H.; Bell, B.; Berrisford, P.; Hirahara, S.; Horányi, A.; Muñoz-Sabater, J.; Nicolas, J.; Peubey, C.; Radu, R.; Schepers, D.; et al. The ERA5 global reanalysis. *Q. J. R. Meteorolog. Soc.* **2020**, *146*, 1999–2049. [CrossRef]
45. Wallace, J.M.; Hobbs, P.V. *Atmospheric Science—An Introductory Survey*, 2nd ed.; Elsevier: New York, NY, USA, 2006; p. 483.
46. American Meteorological Society. Glossary of Meteorology. 2012. Available online: https://glossary.ametsoc.org/wiki/Mixing_ratio (accessed on 8 February 2023).
47. CariCOOS (Caribbean Coastal Ocean Observing System). Weather Flow Mesonet Meteorological Station Aggregation Data. Available online: http://52.55.122.42/thredds/caricoos_mesonet_agg.html (accessed on 13 September 2021).
48. IOOS (Integrated Ocean Observing System). Environmental Sensor Map. Available online: https://sensors.ioos.us/#map (accessed on 18 November 2021).
49. NOAA (National Oceanic and Atmospheric Administration); NCEI (National Centers for Environmental Information). Global Summary of the Day—GSOD. User Engagement and Services Branch. DOC/NOAA/NESDIS/NCDC > National Climatic Data Center, NESDIS, NOAA, U.S. Department of Commerce. Available online: https://www.ncei.noaa.gov/cdo-web/ (accessed on 16 November 2021).
50. WRCC (Western Regional Climate Center). National Interagency Fire Center Remote Automatic Weather Stations (RAWS). Available online: https://raws.dri.edu/prF.html (accessed on 10 November 2021).